Recombinant myonectin ameliorates sepsis-induced cardiomyopathy by alleviating mitochondrial dysfunction via the AdipoR1/AMPK pathway

PEIPEI LI[1], RUI CHEN[2], HANMO ZHANG[3], LIHONG LI[4], HUILING LUO[1], BEIBEI DU[1] and PING YANG[1]

[1]Department of Cardiology, China-Japan Union Hospital of Jilin University, Jilin Provincial Cardiovascular Research Institute, Changchun, Jilin 130031, P.R. China; [2]Cardiovascular Hospital, The First Affiliated Hospital of Zhengzhou University, Zhengzhou University, Zhengzhou, Henan 450052, P.R. China; [3]School of Medicine, Nankai University, Tianjin 300350, P.R. China; [4]Department of Pharmacy, China-Japan Union Hospital of Jilin University, Changchun, Jilin 130031, P.R. China

Received January 31, 2026; Accepted June 2, 2026

DOI: 10.3892/ijmm.2026.5900

Abstract. Sepsis-induced cardiomyopathy (SIC) is a common complication of sepsis and is associated with a high mortality rate; however, effective therapies remain lacking. Mitochondrial dysfunction is a key pathogenic mechanism. Myonectin, also known as C1q tumor necrosis factor-related protein 15, is a novel member of the C1q/TNF-related protein family. It has been demonstrated to exert cardioprotective effects by suppressing inflammatory response, inhibiting apoptosis and attenuating cardiac fibrosis. Despite these known functions, whether myonectin protects against SIC remains unclear. The present study aimed to investigate the protective potential of recombinant myonectin (rMyonectin) against SIC. Lipopolysaccharide (LPS)-induced and cecal ligation and puncture-induced SIC models were established in C57BL/6J mice, and LPS-stimulated neonatal mouse cardiomyocytes (NMCMs) were used for *in vitro* validation. Mice and NMCMs were pretreated with rMyonectin prior to the respective challenge. The results showed that rMyonectin improved cardiac function, attenuated myocardial injury, inhibited apoptosis and preserved the integrity of myocardial mitochondria in SIC mice. Furthermore, rMyonectin inhibited LPS-induced apoptosis in cardiomyocytes. It concurrently promoted mitochondrial biogenesis, maintained mitochondrial dynamics and stabilized mitochondrial membrane potential, thereby improving mitochondrial function and enhancing ATP production. Importantly, these protective effects were abolished by either adiponectin receptor 1 (AdipoR1) knockdown or AMP-activated protein kinase (AMPK) inhibition. These findings suggest that rMyonectin protects against SIC by alleviating mitochondrial dysfunction via the AdipoR1/AMPK pathway, highlighting its promise as a protective agent.

Correspondence to: Dr Beibei Du or Professor Ping Yang, Department of Cardiology, China-Japan Union Hospital of Jilin University, Jilin Provincial Cardiovascular Research Institute, 126 Xiantai Street, Changchun, Jilin 130031, P.R. China
E-mail: beibeidu2012@jlu.edu.cn
E-mail: pyang@jlu.edu.cn

Key words: myonectin, sepsis-induced cardiomyopathy, mitochondrial biogenesis, mitochondrial dynamics, apoptosis

Introduction

Sepsis-induced cardiomyopathy (SIC) is an acute and reversible myocardial dysfunction caused by sepsis. It is clinically characterized by acute systolic and/or diastolic impairment of either one or both ventricles, which is not attributable to coronary artery disease (1). SIC is a relatively common complication of sepsis. Of all patients with sepsis, ~50% exhibit some degree of left or right ventricular dysfunction (2). Patients with SIC have a 2-3 times higher mortality rate than septic patients without cardiac dysfunction (3). Currently, no evidence-based guidelines, effective prevention strategies or specific therapies exist for SIC, representing a major unmet need. Urgent development of novel treatment strategies is key to increasing survival and improving prognoses for these patients.

Sepsis involves multiple pathogenic pathways, including dysregulated inflammatory mediators, mitochondrial dysfunction, oxidative stress and calcium handling abnormalities (4). Bioenergetic and metabolic derangements serve a central role in the development of SIC (5). As the primary energy source of the heart, mitochondria generate the vast majority of ATP required to sustain myocardial contraction (6). Increasing evidence indicates that severe sepsis induces both structural and functional impairments in cardiac mitochondria, resulting in ATP depletion and cardiomyocyte apoptosis (7-10). Thus, mitochondrial-targeted therapy may represent a promising therapeutic strategy for SIC. AMP-activated protein kinase (AMPK), a cellular energy sensor, regulates diverse physiological processes in the cardiovascular system (11). AMPK pathway inhibition was observed in SIC (12,13). In addition to metabolic regulation, AMPK activation also regulates mitochondrial biogenesis and dynamics (fusion-fission) by activating peroxisome proliferator-activated receptor γ co-activator-1α (PGC-1α), thereby enhancing mitochondrial function (11). Adiponectin receptor 1 (AdipoR1) is established

as an upstream activator in the AMPK signaling pathway. Inhibition of the AdipoR1 signaling pathway may lead to myocardial mitochondrial dysfunction and uncoupling (14). This evidence suggests that the AdipoR1/AMPK pathway may serve as a pivotal mediator for promoting mitochondrial function in SIC.

Myonectin, also known as C1q tumor necrosis factor-related protein 15 (CTRP15) or erythroferrone, serves a role in regulating glucose, fatty acid and iron metabolism (15,16). To date, studies on its role in cardiovascular disease remain limited. Otaka *et al* (17) demonstrated that myonectin suppressed inflammatory responses and apoptosis by activating the sphingosine-1-phosphate (S1P)/cAMP/Akt pathway, ameliorating myocardial ischemia-reperfusion (I/R) injury in mice. Another study elucidated that myonectin inhibited cardiac fibrosis through activation of the insulin receptor (IR)/insulin receptor substrate-1 (IRS-1)/Akt signaling pathway (18). These findings suggest that myonectin has a cardioprotective effect. Furthermore, Ozaki *et al* (19) found that myonectin promoted mitochondrial function in skeletal muscle by activating the AMPK/PGC-1α pathway. Whether myonectin can exert cardioprotective effects in SIC by modulating mitochondrial function remains to be elucidated. To address this gap, we hypothesize that myonectin ameliorates SIC by enhancing mitochondrial function through promoting mitochondrial biogenesis and regulating mitochondrial dynamics via the AdipoR1/AMPK pathway. The present study aimed to investigate the protective potential of myonectin against SIC and to elucidate the mechanisms involved.

Materials and methods

Animals and treatments. Male C57BL/6J mice (6-8 weeks old; 20-22 g) were purchased from Jilin Qianhe Model Biotechnology Co., Ltd. During the study period, mice were maintained under specific pathogen-free (SPF) conditions with controlled temperature (20-22˚C) and humidity (45-50%), under a 12-h light/12-h dark cycle. Mice had free access to food and water. All animal experiments were approved by the Institutional Ethics Committee of the School of Basic Medical Sciences, Jilin University (Jilin, China; approval nos. 2025-597 and 2026-491). All procedures were conducted in accordance with the institution's guidelines for the care and use of laboratory animals. To eliminate potential sex-related variability and hormonal fluctuations associated with the estrous cycle, only male mice were included in the present study.

A total of 24 mice were randomly divided into four groups (n=6 per group): Control, control+myonectin, lipopolysaccharide (LPS) and LPS+myonectin groups. Mice in the LPS group received an intraperitoneal injection of LPS (from *E. coli* O111:B4; L2630; MilliporeSigma) at 10 mg/kg to establish a SIC model (20,21). The LPS+myonectin group received a tail vein injection of recombinant mouse myonectin (rMyonectin; cat.no. 00393-06-100; Aviscera Bioscience, Inc.) at 200 ng/g, a dose based on previous literature (17), 2 h before LPS administration. The control group received equal volumes of PBS via tail vein and intraperitoneal injections, separately. The control+myonectin group received rMyonectin at 200 ng/g via tail vein injection, followed by an equal volume of PBS via intraperitoneal injection 2 h later. Cardiac function was assessed by echocardiography 24 h after LPS injection. Subsequently, mice remained deeply anesthetized with an overdose of 5% isoflurane. After the disappearance of corneal reflexes and pedal withdrawal reflexes, which indicated a deep unconscious state, blood was collected via intracardiac puncture, and heart tissues were harvested as an adjunctive means to confirm death. This procedure ensured euthanasia while the animals were unconscious. The total experimental duration was 26 h. Humane endpoints were predefined as meeting any one of the following conditions: Severe respiratory distress evidenced by open-mouth breathing, a decline in body weight >20% relative to baseline, hypothermia (<32˚C), lateral recumbency or loss of responsiveness to external stimuli.

For the cecal ligation and puncture (CLP) model, a total of 24 mice were randomly divided into four groups (n=6 per group): Sham, sham+myonectin, CLP and CLP+myonectin groups. The experimental procedure for CLP was based on previously published literature (22,23). Mice were anesthetized with isoflurane (4% for induction and 2% for maintenance). Following disinfection of the lower abdomen with 75% ethanol, a 1.5 cm midline longitudinal incision was made to expose the cecum. The distal three-quarters of the cecum was ligated. A total of two holes were then punctured in the ligated segment using a 22-gauge needle, and a small amount of fecal content was gently expressed. The cecum was subsequently returned to the peritoneal cavity, and the abdominal incision was closed in layers with sutures. Immediately after surgery, 1 ml sterile saline was administered intraperitoneally to compensate for fluid loss. Sham-operated mice were subjected to the identical surgical procedure except that CLP was omitted. No antibiotics were administered during the experimental period. The sham+myonectin and the CLP+myonectin groups were pretreated with rMyonectin (200 ng/g) via tail vein injection 2 h prior to the procedure. Cardiac function was assessed by echocardiography 24 h after surgery. The total experimental duration was 26 h. The procedures for anesthesia, euthanasia and blood and tissue collection, as well as the humane endpoints, were identical to those described for the LPS model.

To determine the survival rate, separate experiments were conducted. For the LPS model, mice were randomly divided into four groups (n=10 per group): Control, control+myonectin, LPS and LPS+myonectin groups. For the CLP model, mice were randomly divided into four groups (n=10 per group): Sham, sham+myonectin, CLP and CLP+myonectin groups. Mice were pretreated via tail vein injection with either rMyonectin (200 ng/g) or PBS 2 h prior to an intraperitoneal dose of LPS (15 mg/kg) or CLP surgery. Survival was monitored every 12 h for 3 days as described previously (24,25).

A total of 128 mice were used in the present study, of which 123 were euthanized, while 5 were found dead (attributed to SIC-mediated cardiac emergencies). Of the 123 mice that were euthanized, 24 were euthanized upon reaching humane endpoints, and the remaining 99 were euthanized at the scheduled end of the study.

Echocardiographic assessment. Echocardiography was performed under isoflurane anesthesia (4% for induction and 2% for maintenance) in mice from each group using a GE Vivid E95 ultrasound system (GE Healthcare Technologies, Inc.) to

non-invasively evaluate changes in cardiac structure and function. M-mode images were acquired from the left ventricular long-axis view, and left ventricular parameters including left ventricular ejection fraction (LVEF), left ventricular fractional shortening (LVFS), left ventricular internal diameter at end-systole (LVIDs), left ventricular internal diameter at end-diastole (LVIDd) and heart rate (HR) were measured. The echocardiographer was blinded to the treatment groups.

Histological analysis. Cardiac tissues were fixed in 4% paraformaldehyde at 4˚C for 48 h, embedded in paraffin and sectioned at 4-μm thickness. Sections were deparaffinized with dimethylbenzene and rehydrated through a graded ethanol series (100, 95, 80 and 70%). Subsequently, parallel sections were processed for hematoxylin and eosin (H&E) staining and terminal deoxynucleotidyl transferase dUTP nick end labeling (TUNEL) assay. The stained sections were observed and imaged under the microscope (OLYMPUS BX53), and the images were analyzed using ImageJ software (National Institutes of Health; v1.54f). The apoptotic index was calculated as the integrated density of TUNEL-positive cells divided by the total DAPI-stained nuclear area.

ATP assessment. The relative levels of ATP were determined using the ATP assay kit (cat. no. S0027; Beyotime Biotechnology) according to the manufacturer's instructions. Samples (20 mg cardiac tissue or cells from one well of a 6-well plate) were homogenized with ATP lysis buffer (200 μl). Cell lysates or tissue homogenates were centrifuged at 12,000 x g for 5 min at 4˚C, and the supernatants were collected and kept on ice. ATP working solution (100 μl) was added to each well of 96-well plates and allowed to equilibrate at room temperature for 3-5 min. Subsequently, 20 μl sample or standard solution was added to each well and mixed thoroughly. The values, relative light unit (RLU), were measured using the multimode microplate reader (CLARIOSTAR, BMG Labtech GmbH).

Enzyme-linked immunosorbent assay (ELISA). Serum was obtained by centrifugation (1,000 x g; 15 min; 4˚C) of blood samples after allowing them to clot at room temperature for 2 h. The levels of cardiac troponin I (cTn-I) and brain natriuretic peptide (BNP) in the serum were measured using the commercial ELISA kits (cat. nos. CSB-E08421m and CSB-E07971m; Cusabio Technology, LLC) according to the manufacturer's instructions.

Transmission electron microscopy (TEM). Mitochondrial ultrastructure was observed using TEM. Heart tissue was initially fixed in 3% glutaraldehyde overnight at 4˚C, post-fixed in 1% osmium tetroxide for 2 h at 4˚C and rinsed with PBS. Following dehydration through a graded ethanol series, the samples were embedded in Epon resin. Ultrathin sections (50 nm) were cut using a diamond knife and mounted on copper grids. The sections were then stained with uranyl acetate for 15 min at room temperature and lead citrate for 10 min at room temperature. Images were acquired using the TEM (Hitachi H600 Electron Microscope, Hitachi, Ltd.) at magnifications of x3,000, x7,000 and x20,000 to assess overall morphology and detailed structures.

Isolation and culture of neonatal mouse cardiomyocytes (NMCMs). The isolation and culture of NMCMs were performed based on a previously described method (26). Neonatal C57BL/6J mice (1-3 days old) were derived from an in-house SPF breeding colony established by mating male and female mice purchased from Jilin Qianhe Model Biotechnology Co., Ltd. Following anesthesia induction with 2% isoflurane (on a thermostatic heating pad at 37˚C for ~2 min) and confirmation of loss of consciousness and reflexes, mice were euthanized by rapid decapitation with sterile scissors, and hearts were aseptically harvested, promptly chilled, washed, and minced in cold Ca^{2+}- and Mg^{2+}-free Hank's Balanced Salt Solution (cat. no. 14175095; Gibco; Thermo Fisher Scientific, Inc.). The tissue fragments were then digested in a solution of 1 mg/ml trypsin (cat. no. T4799; MilliporeSigma) at 4˚C for 7 h. The trypsin solution was then removed. The tissue fragments were subjected to sequential digestions with 0.8 mg/ml Collagenase Type II (cat. no. C6885; MilliporeSigma) in a 37˚C water bath for 5 min per cycle, until no visible tissue fragments remained. The released cell suspension from each digestion was collected and kept on ice. The cell suspension was centrifuged at 200 x g for 5 min at 4˚C. The pellet was resuspended in Dulbecco's modified Eagle medium/F12 Ham medium (DMEM/F12; cat. no. C11330500BT; Gibco; Thermo Fisher Scientific, Inc.) supplemented with 10% Fetal Bovine Serum (FBS; cat. no. A5256701; Gibco; Thermo Fisher Scientific, Inc.) and 1% penicillin-streptomycin solution. The cell suspension was filtered through a cell strainer and cultured for 90 min under standard culture conditions (37˚C, 5% CO_2) to remove fibroblasts. Cardiomyocytes were then collected, plated onto culture dishes pre-coated with 0.01% poly-L-lysine (cat. no. ST508; Beyotime Biotechnology) and cultured until a synchronous, spontaneous beating rhythm was observed, after which they were ready for subsequent treatments. NMCMs were pretreated for 2 h with rMyonectin or with the AMPK inhibitor Compound C (CC; 10 μM; cat. no. HY-13418A; MedChemExpress) (27,28), followed by stimulation with 10 μg/ml LPS for 24 h (29).

Small interfering (si)RNA interference. The AdipoR1-targeting siRNA was designed and synthesized by GenCefe Biotech and had the following sequences: Sense strand, 5'-GGCUCUUCC ACACUGUCUTT-3'; antisense strand, 5'-UAGACAGUGUGG AAGAGCCTT-3'. The negative control siRNA sequences were: Sense strand, 5'-UUCUCCGAACGUGUCACGUTT-3'; antisense strand, 5'-ACGUGACACGUUCGGAGAATT-3'. Cells were transfected with 150 pmol siRNA per well in a 6-well plate using 7.5 μl GP-transfect-Mate reagent (cat. no. G04008; Shanghai GenePharma Co., Ltd.). After 6 h incubation at 37˚C, the medium was replaced with fresh culture medium, and the cells were further cultured. The levels of mRNA and protein were assessed at 24 and 48 h, respectively.

Cell counting kit-8 (CCK-8) assay. Cell viability of NMCMs was assessed using the CCK-8 assay (cat. no. BA00208; Bioss) according to the manufacturer's instructions. Absorbance was measured at 450 nm.

Intracellular lactate dehydrogenase (LDH) activity assay. The activity of intracellular LDH was determined with the

commercial assay kit (cat. no. BC0685; Beijing Solarbio Science & Technology Co., Ltd.) per the manufacturer's instructions. Cells were lysed in the provided extraction buffer and sonicated on ice. After centrifugation of the lysates (8,000 x g; 10 min; 4˚C), the absorbance of the supernatant was measured at 450 nm. The protein concentration of the supernatant was determined using a BCA Protein Assay Kit (cat. no. C05-02001; Bioss) to normalize the LDH activity. Finally, the specific activity of LDH was calculated and expressed as units per milligram of protein.

Mitochondrial membrane potential (MMP) assessment. MMP was evaluated using a JC-1 assay kit (cat. no. C2003S; Beyotime Biotechnology) following the manufacturer's instructions. NMCMs were plated on glass-bottom confocal culture dishes and stained with 1 μM JC-1 probes for 20 min at 37˚C in the dark. After washing twice with PBS, fluorescent images were immediately acquired using the confocal microscope (Nikon Corporation). The fluorescent signals of JC-1 aggregates (red) and monomers (green) were recorded. The ratio of red-to-green fluorescence intensity was quantified using ImageJ software (National Institutes of Health, v1.54f) to evaluate MMP.

Mitochondrial respiratory chain complex I and III activity assay. The activities of mitochondrial respiratory chain complexes I and III were assessed using the Cell Mitochondrial Complex I (NADH-CoQ Reductase) Activity Assay Kit (cat. no. E-BC-K834-M; Wuhan Elabscience Biotechnology Co., Ltd.) and the Cell Mitochondrial Complex III (Coenzyme Q-Cytochrome C Reductase) Activity Assay Kit (cat. no. E-BC-K836-M; Wuhan Elabscience Biotechnology Co., Ltd.), respectively. Cardiomyocytes were harvested, resuspended in the provided extraction solution and processed according to the manufacturer's instructions for mitochondrial respiratory chain complex extraction. The absorbance was measured at 340 nm (for complex I) and 550 nm (for complex III).

Measurement of oxygen consumption rate (OCR). After treatment according to the experimental groups, cells were cultured for 24 h. OCR was evaluated using the Enhanced Oxygen Consumption Rate Fluorometric Assay Kit (cat. no. E-BC-F070; Wuhan Elabscience Biotechnology Co., Ltd.). The microplate was placed in the multifunctional microplate reader (Synergy H1, BioTek; Agilent Technologies, Inc.) set at 37˚C in dynamic reading mode. The excitation wavelength was set at 405 nm, the emission wavelength at 675 nm, and measurements were taken every 2 min for 100 min. Finally, the fluorescence values were plotted against time, and OCR was represented by the slopes of the curves.

Flow cytometry. Cell apoptosis was analyzed using flow cytometry. Following harvest by trypsinization, cells were stained with Annexin V-FITC and propidium iodide (PI), and then immediately analyzed by a DxFLEX flow cytometer (Beckman Coulter, Inc.). The data were analyzed using FlowJo software (v10.8.1; BD Biosciences) to quantify the percentage of apoptotic cells in each group.

Western blot. Proteins were extracted from cardiac tissue and NMCMs using RIPA lysis buffer (cat. no. PC101; Shanghai Epizyme Biopharmaceutical Technology Co., Ltd.) supplemented with protease and phosphatase inhibitors. The protein concentration was quantified with the BCA Protein Assay Kit (cat. no. C05-02001; Bioss). Equal amounts of proteins (20 μg per lane) were denatured in SDS-PAGE loading buffer (cat. no. P1040; Beijing Solarbio Science & Technology Co., Ltd.) at 100˚C for 5 min, separated by 8-12% SDS-PAGE and transferred to PVDF membranes. The membranes were blocked with 5% skim milk for 1 h at room temperature and then incubated overnight at 4˚C with the following primary antibodies: Bax (1:1,000; cat. no. ab32503; Abcam), Bcl-2 (1:1,000; cat. no. A19693; ABclonal Biotech Co., Ltd.), cleaved caspase-3 (1:600; cat. no. WL02117; Wanleibio Co., Ltd.), caspase-3 (1:500; cat. no. T40044; Abmart Pharmaceutical Technology Co., Ltd.), PGC-1α (1:2,000; cat. no. ab313559; Abcam), nuclear respiratory factor 1 (NRF1; 1:1,000; cat. no. A3252; ABclonal Biotech Co., Ltd.), mitochondrial transcription factor A (TFAM; 1:1,000; cat. no. 15218; Cell Signaling Technology, Inc.), mitofusin 2 (Mfn2; 1:3,000; cat. no. ab124773; Abcam), optic atrophy 1 (OPA1; 1:1,000; cat. no. ab157457; Abcam), phosphorylated (p)-dynamin-related protein 1 (Drp1; Ser616; 1:1,000; cat. no. ab314755; Abcam), Drp1 (1:4,000; cat. no. ab184247; Abcam), p-AMPK (1:1,000; cat. no. ab133448; Abcam), AMPK (1:1,000; cat. no. ab207442; Abcam), AdipoR1 (1:4,000; cat. no. bs-0610R; Bioss), β-actin (1:8,000; cat. no. P30002; Abmart Pharmaceutical Technology Co., Ltd.) and β-tubulin (1:10,000; cat. no. A12289; ABclonal Biotech Co., Ltd.). After washing, the membranes were incubated with HRP-conjugated Goat Anti-Rabbit secondary antibody (1:10,000; cat. no. ab6721; Abcam) for 1 h at room temperature. After incubation with an enhanced chemiluminescence (ECL) substrate, the bands were visualized using MiniChemi 610 System (SinSage Technology, Co., Ltd.) and SageCapture™ software. Band intensities were quantified using ImageJ software (National Institutes of Health, v1.54f) and normalized to β-actin or β-tubulin.

Reverse transcription-quantitative PCR (RT-qPCR) analysis. Total RNA was extracted using the Fast Total RNA Extraction Kit (cat. no. RP1201; BioTeke Corporation). cDNA was synthesized from the extracted RNA with the ToloScript All-in-One RT EasyMix for qPCR (cat. no. 22107-01; Tolo Biotech Co., Ltd.) according to the manufacturer's instructions. The primers were synthesized by Comate Bioscience. The primer sequences used in the present study were as follows: AdipoR1: Forward 5'-GAGAAGATGGAGGAGTTCGTGTA-3', reverse 5'-AGC AGGTAGTCGTTGTCTTTCAG-3'; β-actin: Forward 5'-GTA CTCTGTGTGGATCGGTGG-3', reverse 5'-GCAGCTCAG TAACAGTCCG-3'. Following the mixture of cDNA, primers, and the 2X Q3 SYBR qPCR Master Mix (cat. no. 22204; Tolo Biotech Co., Ltd.), qPCR was performed using the Real-Time PCR system (ABI 7500 DX). The thermocycling protocol was as follows: Initial denaturation at 95˚C for 30 sec, followed by 40 cycles of 95˚C for 10 sec and 60˚C for 30 sec. A melt curve analysis was performed to verify amplification specificity. Relative gene expression was quantified via the $2^{-\Delta\Delta Cq}$ method (30), where β-actin served as internal control.

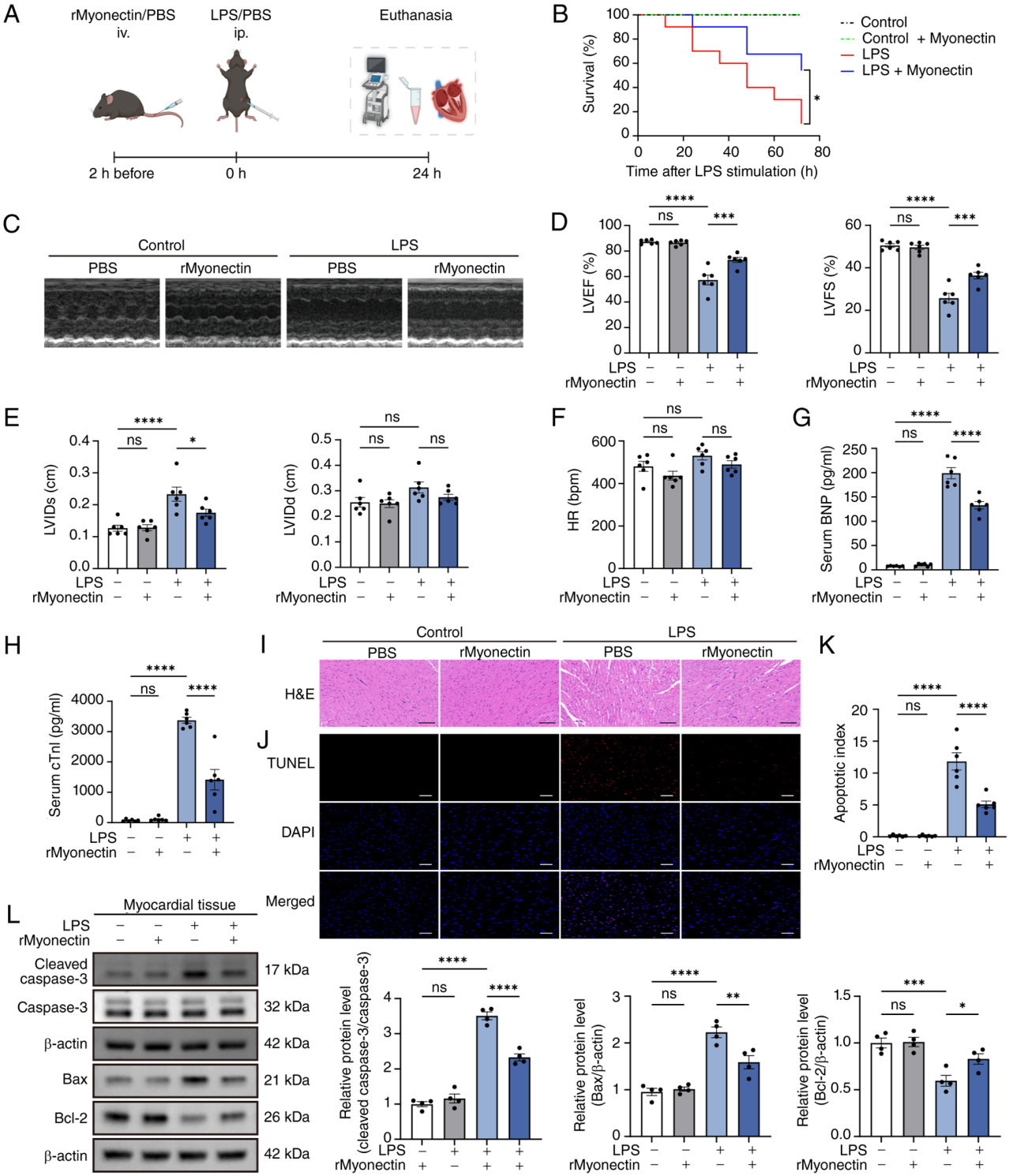

Figure 1. rMyonectin improves cardiac function, attenuates myocardial injury and inhibits apoptosis in LPS-induced sepsis-induced cardiomyopathy mice. (A) Schematic diagram of the timeline for LPS and rMyonectin administration and subsequent cardiac evaluation. (B) Survival curves. (C) Representative images from echocardiography. (D) LVEF and LVFS. (E) LVIDs and LVIDd. (F) HR. The serum levels of (G) BNP and (H) cTn-I. (I) H&E staining of heart sections. Scale bar, 100 μm. (J) TUNEL assay of heart sections. Scale bar, 50 μm. (K) Quantification of apoptosis in TUNEL-stained sections. (L) Western blot analysis and semi-quantification of cleaved caspase-3, caspase-3, Bax and Bcl-2 protein expression in myocardial tissue. The data are presented as mean±SEM. *P<0.05, **P<0.01, ***P<0.001, ****P<0.0001. The schematic diagram was created using BioRender.com. rMyonectin, recombinant myonectin; LVEF, left ventricular ejection fraction; LVFS, left ventricular fractional shortening; LVIDs, left ventricular internal diameter at end-systole; LVIDd, left ventricular internal diameter at end-diastole; HR, heart rate; BNP, brain natriuretic peptide; cTn-I, cardiac troponin I; TUNEL, terminal deoxynucleotidyl transferase dUTP nick end labeling; LPS, lipopolysaccharide; H&E, hematoxylin and eosin.

Statistical analysis. Data from three or more independent experiments are presented as the mean±SEM. Statistical analyses were performed using GraphPad Prism software (version 10.0; Dotmatics). Comparisons among multiple groups were performed using one-way ANOVA followed by Tukey's multiple comparison test. Survival was assessed

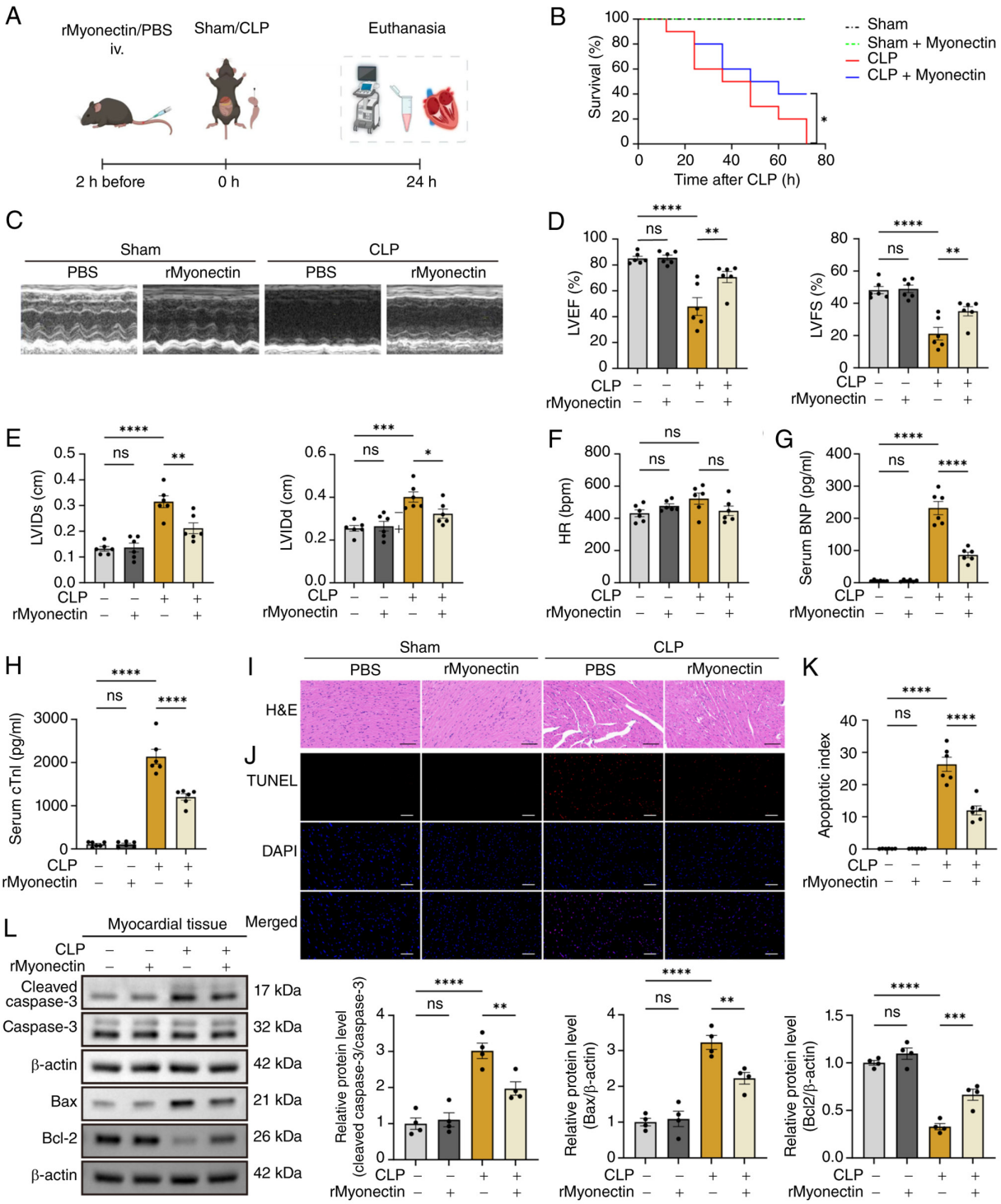

Figure 2. rMyonectin improves cardiac function, attenuates myocardial injury and inhibits apoptosis in CLP-induced sepsis-induced cardiomyopathy mice. (A) Schematic diagram of the timeline for CLP surgery and rMyonectin administration, and subsequent cardiac evaluation. (B) Survival curves. (C) Representative images from echocardiography. (D) LVEF and LVFS. (E) LVIDs and LVIDd. (F) HR. The serum levels of (G) BNP and (H) cTn-I. (I) H&E staining of heart sections. Scale bar, 100 μm. (J) TUNEL assay of heart sections. Scale bar, 50 μm. (K) Quantification of apoptosis in TUNEL-stained sections. (L) Western blot analysis and semi-quantification of cleaved caspase-3, caspase-3, Bax, and Bcl-2 protein expression in myocardial tissue. The data are presented as mean±SEM. *P<0.05, **P<0.01, ***P<0.001, ****P<0.0001. The schematic diagram was created using BioRender.com. rMyonectin, recombinant myonectin; CLP, cecal ligation and puncture; LVEF, left ventricular ejection fraction; LVFS, left ventricular fractional shortening; LVIDs, left ventricular internal diameter at end-systole; LVIDd, left ventricular internal diameter at end-diastole; HR, heart rate; BNP, brain natriuretic peptide; cTn-I, cardiac troponin I; TUNEL, terminal deoxynucleotidyl transferase dUTP nick end labeling; H&E, hematoxylin and eosin.

using the Kaplan-Meier method, and differences between groups were compared with the Gehan-Breslow-Wilcoxon test. P<0.05 was considered to indicate a statistically significant difference.

Results

rMyonectin improves cardiac function, attenuates myocardial injury and inhibits apoptosis in SIC mice. Following

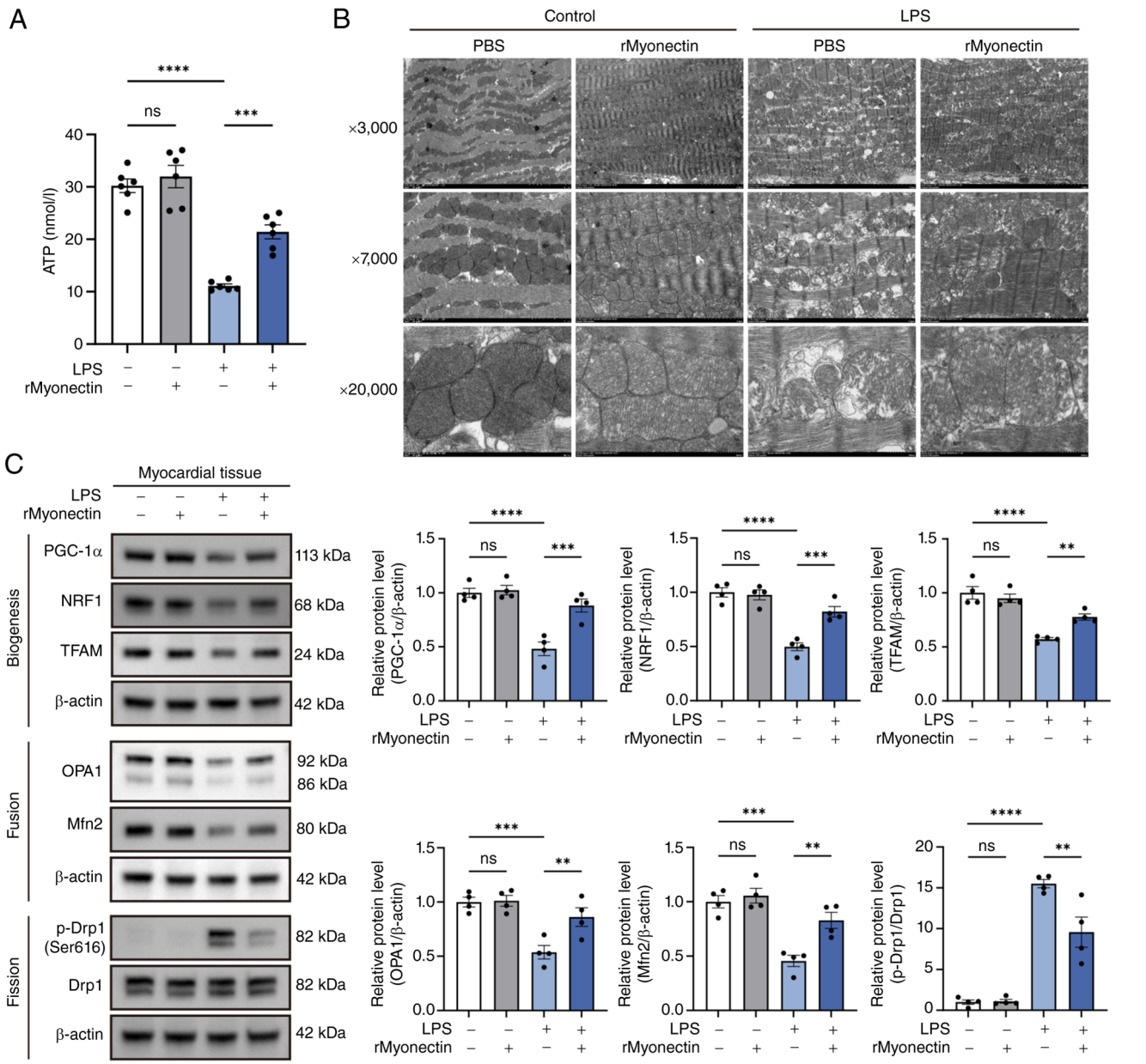

Figure 3. rMyonectin protects cardiac mitochondria in LPS-induced sepsis-induced cardiomyopathy mice by promoting mitochondrial biogenesis and maintaining mitochondrial dynamics. (A) The ATP content in myocardial tissue. (B) Mitochondrial ultrastructure of myocardial tissue was observed by TEM. Magnification, x3,000, x7,000 and x20,000. (C) Western blot analysis and semi-quantification of PGC-1α, NRF1, TFAM, OPA1, Mfn2, p-Drp1 at Ser616 and Drp1 in myocardial tissue. The data are presented as mean±SEM. **P<0.01, ***P<0.001, ****P<0.0001. rMyonectin, recombinant myonectin; TEM, transmission electron microscopy; PGC-1α, peroxisome proliferator-activated receptor γ co-activator-1 α; NRF1, nuclear respiratory factor 1; TFAM, mitochondrial transcription factor A; Mfn2, mitofusin 2; OPA1, optic atrophy 1; Drp1, dynamin-related protein 1; LPS, lipopolysaccharide; p-, phosphorylated.

pretreatment with rMyonectin via tail vein injection, SIC was induced in mice by intraperitoneal injection of LPS after a 2-h interval. Cardiac function was evaluated by echocardiography 24 h post-induction. Subsequently, blood samples and heart tissue were collected under anesthesia for analysis (Fig. 1A). The results showed that rMyonectin administration significantly improved the survival rate of mice challenged with LPS (Fig. 1B). Echocardiographic assessment revealed that LPS-challenged mice displayed significant impairments in cardiac systolic function compared with controls, characterized by reduced LVEF and LVFS, alongside increased LVIDs (Fig. 1C-F). Consistent with these functional deficits, serum levels of BNP and cTn-I were markedly elevated in LPS-challenged mice (Fig. 1G and H), confirming the successful induction of SIC. Notably, pretreatment with rMyonectin effectively attenuated these pathophysiological alterations, improving systolic performance and reducing myocardial injury (Fig. 1C-H). Histopathological analysis revealed that myocardial fibers in the control group were orderly arranged with preserved interstitial integrity. rMyonectin treatment alone induced no structural alterations. By contrast, LPS challenge induced distinct pathological changes, including cardiomyocyte disarray, interstitial edema and vacuolar degeneration. Importantly, rMyonectin pretreatment significantly attenuated these LPS-induced structural abnormalities (Fig. 1I). Furthermore, rMyonectin significantly

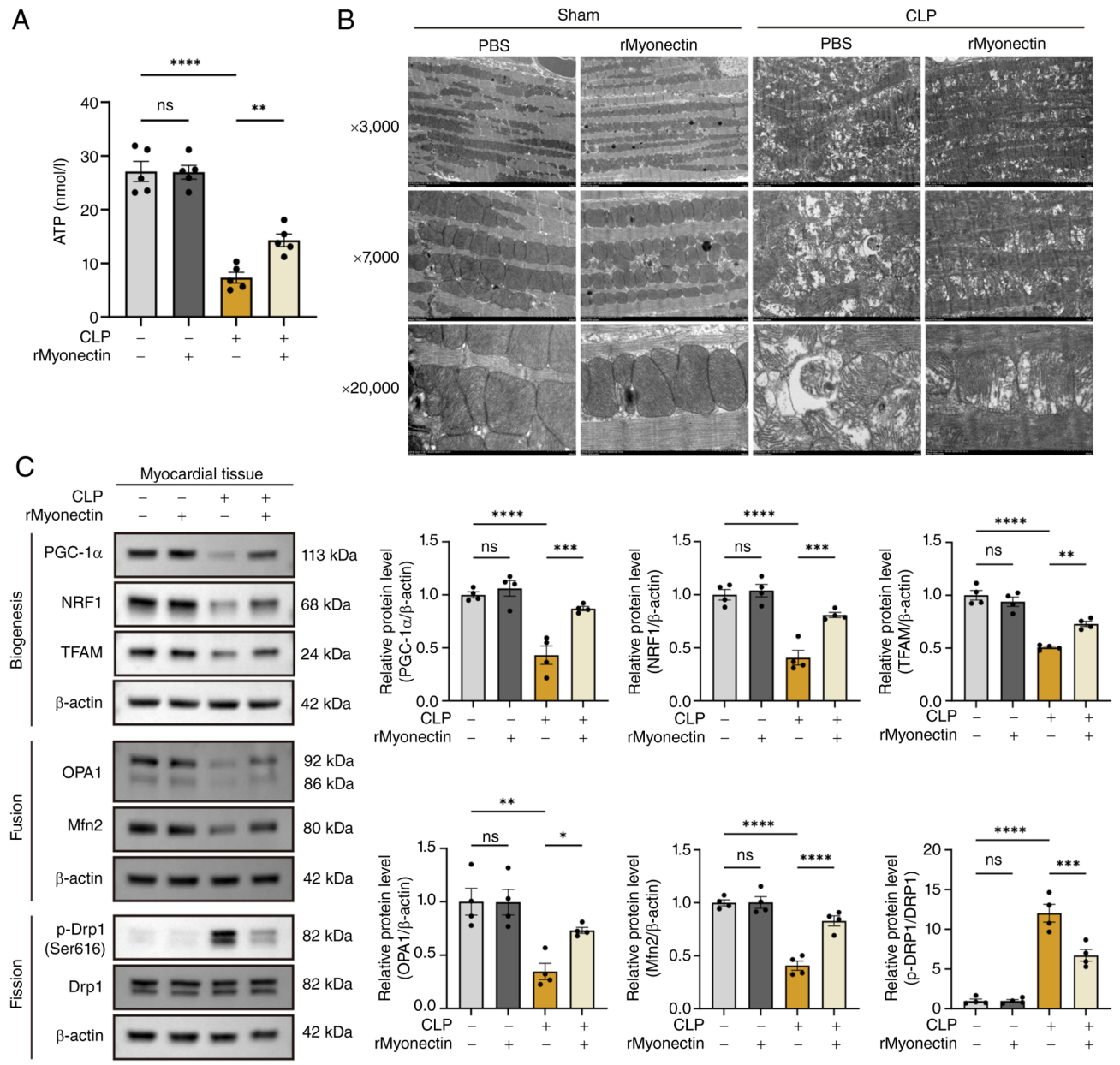

Figure 4. rMyonectin protects cardiac mitochondria in CLP-induced sepsis-induced cardiomyopathy mice by promoting mitochondrial biogenesis and maintaining mitochondrial dynamics. (A) The ATP content in myocardial tissue. (B) Mitochondrial ultrastructure of myocardial tissue was observed by TEM. Magnification, x3,000, x7,000 and x20,000. (C) Western blot analysis and semi-quantification of PGC-1α, NRF1, TFAM, OPA1, Mfn2, p-Drp1 at Ser616 and Drp1 in myocardial tissue. The data are presented as mean±SEM. *P<0.05, **P<0.01, ***P<0.001, ****P<0.0001. rMyonectin, recombinant myonectin; CLP, cecal ligation and puncture; TEM, transmission electron microscopy; PGC-1α, peroxisome proliferator-activated receptor γ co-activator-1 α; NRF1, nuclear respiratory factor 1; TFAM, mitochondrial transcription factor A; Mfn2, mitofusin 2; OPA1, optic atrophy 1; Drp1, dynamin-related protein 1; p-, phosphorylated.

attenuated LPS-induced cardiomyocyte apoptosis, as shown by a reduced apoptosis index (Fig. 1J and K), downregulated cleaved caspase-3 and Bax, and upregulated Bcl-2 in myocardial tissue (Fig. 1L).

Moreover, a CLP-induced model was established in C57BL/6J mice to further evaluate the effects of rMyonectin on SIC (Fig. 2A). The results showed that rMyonectin significantly improved the survival rate (Fig. 2B), ameliorated cardiac dysfunction (Fig. 2C-G) and myocardial injury (Fig. 2H and I), and inhibited cardiomyocyte apoptosis (Fig. 2J-L) in CLP-induced SIC mice. These results demonstrate that rMyonectin protects against SIC irrespective of the sepsis model, whether endotoxemic or polymicrobial.

rMyonectin protects cardiac mitochondria in SIC mice by promoting mitochondrial biogenesis and maintaining mitochondrial dynamics. The present study revealed that rMyonectin attenuated the LPS-induced decrease in myocardial ATP levels (Fig. 3A). This indicated a beneficial role for myonectin in cardiac energy metabolism during SIC. Due to the central role of mitochondria in cardiac energetics, their morphology was assessed using TEM. Results revealed that LPS challenge induced mitochondrial shortening, swelling, cristae disruption and increased vacuolation. These structural defects were mitigated by rMyonectin pretreatment (Fig. 3B). At the molecular level, relative to LPS administration alone, pretreatment with rMyonectin upregulated the expression of

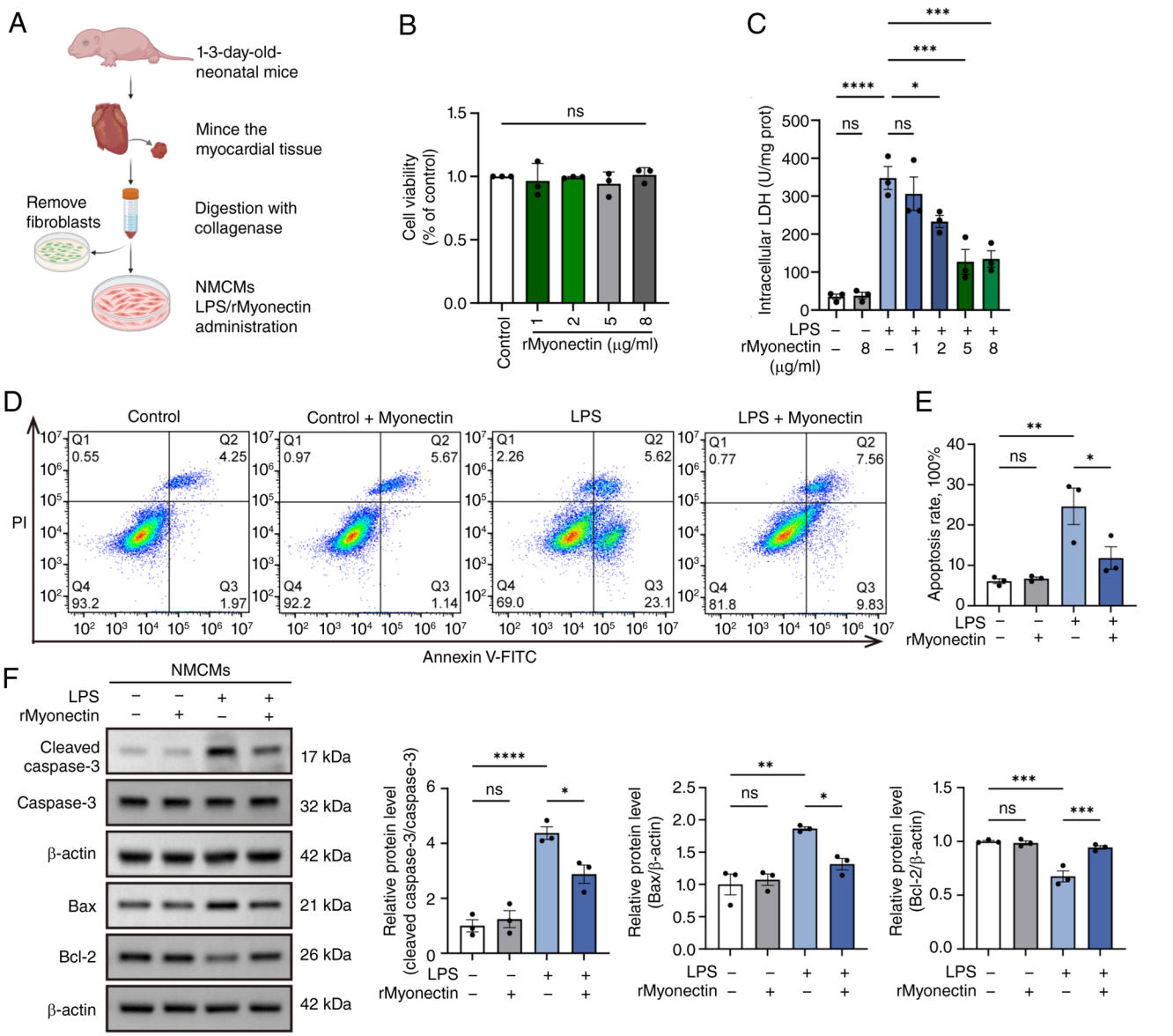

Figure 5. rMyonectin attenuates LPS-induced cardiomyocyte injury and inhibits apoptosis. (A) Schematic diagram showing the isolation and culture of NMCMs. NMCMs were pretreated for 2 h with rMyonectin, followed by stimulation with LPS for 24 h. (B) Cell viability of NMCMs was determined by Cell Counting Kit-8 assay after 24-h treatment with increasing concentrations of rMyonectin (1, 2, 5, 8 μg/ml). (C) Intracellular LDH activity in NMCMs pretreated with rMyonectin (1, 2, 5, 8 μg/ml) prior to LPS stimulation. (D) Apoptosis was assessed by flow cytometry after double labeling with Annexin V-FITC and PI. (E) The percentage of apoptotic cells detected using flow cytometry. (F) Western blot analysis and semi-quantification of cleaved caspase-3, caspase-3, Bax and Bcl-2 protein expression in NMCMs. The data are presented as mean±SEM. *P<0.05, **P<0.01, ***P<0.001, ****P<0.0001. The schematic diagram was created using BioRender.com. rMyonectin, recombinant myonectin; NMCMs, neonatal mouse cardiomyocytes; LDH, lactate dehydrogenase; LPS, lipopolysaccharide; PI, propidium iodide.

PGC-1α, NRF1, TFAM, OPA1 and Mfn2 while reducing the p-Drp1(Ser616)/Drp1 ratio, thereby promoting mitochondrial biogenesis and restoring the balance of mitochondrial fusion-fission dynamics (Fig. 3C). Consistently, in CLP-induced SIC mice, rMyonectin pretreatment also attenuated myocardial ATP depletion (Fig. 4A), improved mitochondrial ultrastructure (Fig. 4B), promoted mitochondrial biogenesis and restored the balance of mitochondrial fusion-fission dynamics (Fig. 4C).

rMyonectin attenuates LPS-induced cardiomyocyte injury and inhibits apoptosis. NMCMs were isolated from 1-3-day-old C57BL/6J mice and treated with LPS to establish an *in vitro* model of SIC (Fig. 5A). To evaluate the cellular safety of rMyonectin, NMCMs were treated with increasing concentrations of rMyonectin (1, 2, 5 and 8 μg/ml). The CCK-8 assay showed that rMyonectin at these concentrations had no significant effect on cell viability (Fig. 5B). To assess its protective effect, NMCMs were pretreated with the same concentrations of rMyonectin prior to LPS challenge. Analysis revealed that rMyonectin reduced the activity of LPS-induced intracellular LDH. Notably, LDH activity was significantly reduced at a concentration of 5 μg/ml, but no further reduction was observed at 8 μg/ml (Fig. 5C). Therefore, 5 μg/ml rMyonectin was selected for subsequent experiments. At this optimal concentration,

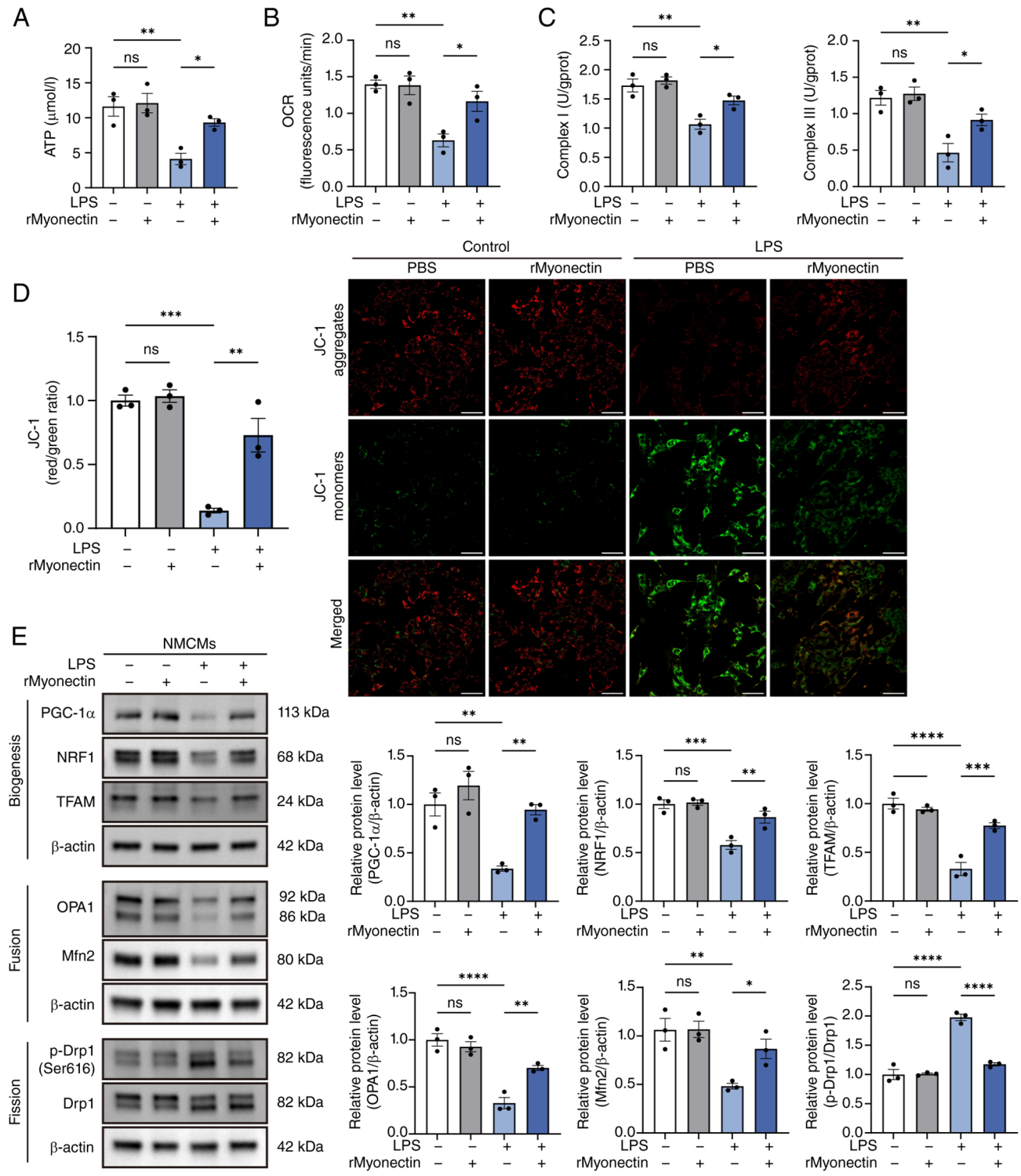

Figure 6. rMyonectin ameliorates LPS-induced mitochondrial dysfunction in cardiomyocytes. (A) The ATP content in NMCMs. (B) Relative OCR. (C) Detection of the activities of mitochondrial respiratory chain complexes I and III. (D) Analysis of MMP using JC-1 staining. Scale bar, 50 μm. (E) Western blot analysis and semi-quantification of PGC-1α, NRF1, TFAM, OPA1, Mfn2, p-Drp1 at Ser616, and Drp1 in NMCMs. The data are presented as mean±SEM. *P<0.05, **P<0.01, ***P<0.001, ****P<0.0001. rMyonectin, recombinant myonectin; NMCMs, neonatal mouse cardiomyocytes; OCR, oxygen consumption rate; MMP, mitochondrial membrane potential; PGC-1α, peroxisome proliferator-activated receptor γ co-activator-1 α; NRF1, nuclear respiratory factor 1; TFAM, mitochondrial transcription factor A; Mfn2, mitofusin 2; OPA1, optic atrophy 1; Drp1, dynamin-related protein 1; LPS, lipopolysaccharide; p-, phosphorylated.

rMyonectin pretreatment reduced LPS-induced apoptosis (Fig. 5D and E) and downregulated cleaved caspase-3 and Bax, while upregulating Bcl-2 expression (Fig. 5F). Taken together, these data indicate that rMyonectin attenuates LPS-induced cardiomyocyte injury and inhibits apoptosis.

rMyonectin ameliorates LPS-induced mitochondrial dysfunction in cardiomyocytes. In cardiomyocytes, rMyonectin reversed the LPS-induced decrease in ATP levels (Fig. 6A), ameliorated the reductions in OCR (Fig. 6B) and in the activities of mitochondrial respiratory chain complexes I and III (Fig. 6C), and

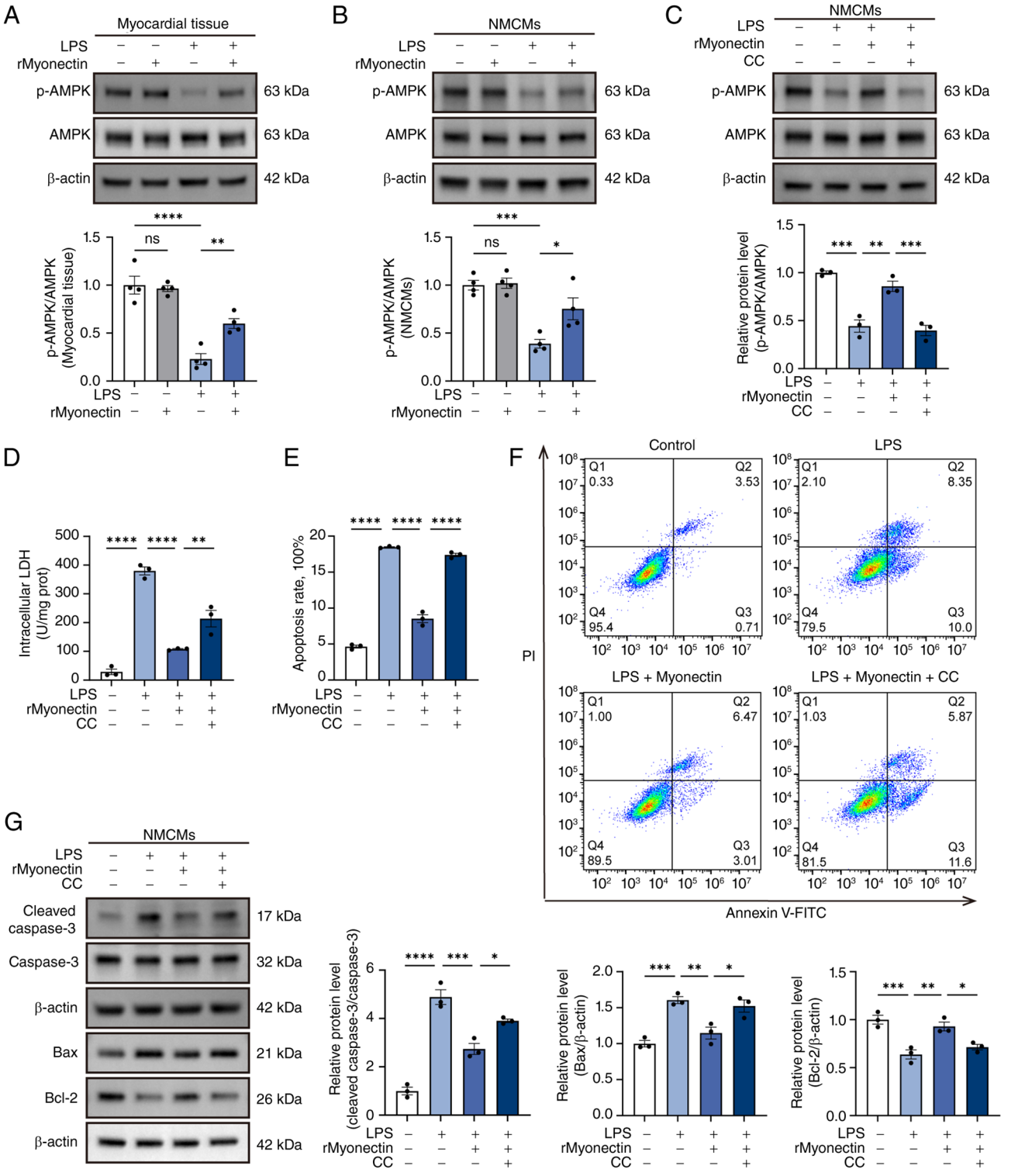

Figure 7. Protective effect of rMyonectin against LPS-induced apoptosis in cardiomyocytes is mediated by AMPK activation. (A) Western blot analysis and semi-quantification of p-AMPK and AMPK in myocardial tissue. (B) Western blot analysis and semi-quantification of p-AMPK and AMPK in NMCMs. (C) Expression of p-AMPK and AMPK in NMCMs after CC treatment. (D) Intracellular LDH activity in NMCMs. (E) The percentage of apoptotic cells detected using flow cytometry. (F) Apoptosis was assessed using flow cytometry after double labeling with Annexin V-FITC and PI. (G) Western blot analysis and semi-quantification of cleaved caspase-3, caspase-3, Bax and Bcl-2 protein expression in NMCMs. The data are presented as mean±SEM. *P<0.05, **P<0.01, ***P<0.001, ****P<0.0001. rMyonectin, recombinant myonectin; NMCMs, neonatal mouse cardiomyocytes; AMPK, AMP-activated protein kinase; CC, Compound C; LDH, lactate dehydrogenase; LPS, lipopolysaccharide; PI, propidium iodide; p-, phosphorylated.

stabilized MMP (Fig. 6D). Consistent with the *in vivo* observations, LPS challenge downregulated PGC-1α, NRF1, TFAM, OPA1 and Mfn2 while increasing the p-Drp1(Ser616)/Drp1 ratio, all of which were reversed by rMyonectin (Fig. 6E). These results indicate that rMyonectin ameliorates LPS-induced mitochondrial dysfunction, as evidenced by enhanced mitochondrial respiratory function, stabilized membrane potential, and restored mitochondrial dynamics and biogenesis.

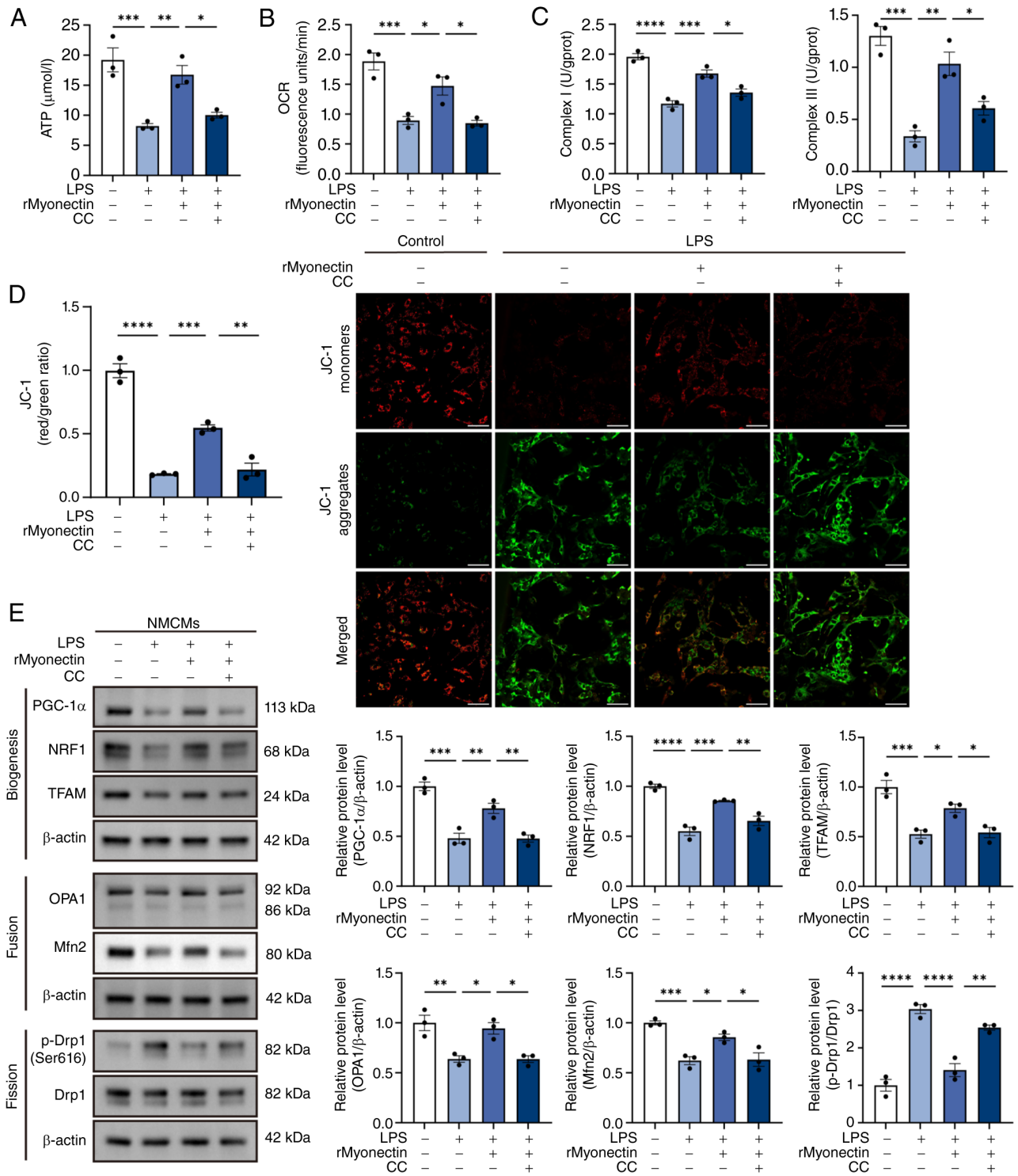

Figure 8. Protective effect of rMyonectin against LPS-induced mitochondrial dysfunction in cardiomyocytes is mediated by AMPK activation. (A) The ATP content in NMCMs. (B) Relative OCR. (C) Detection of the activities of mitochondrial respiratory chain complexes I and III. (D) Analysis of MMP using JC-1 staining. Scale bar, 50 μm. (E) Western blot analysis and semi-quantification of PGC-1α, NRF1, TFAM, OPA1, Mfn2, p-Drp1 at Ser616, and Drp1 in NMCMs. The data are presented as mean±SEM. *P<0.05, **P<0.01, ***P<0.001, ****P<0.0001. rMyonectin, recombinant myonectin; NMCMs, neonatal mouse cardiomyocytes; OCR, oxygen consumption rate; MMP, mitochondrial membrane potential; PGC-1α, peroxisome proliferator-activated receptor γ co-activator-1 α; NRF1, nuclear respiratory factor 1; TFAM, mitochondrial transcription factor A; Mfn2, mitofusin 2; OPA1, optic atrophy 1; Drp1, dynamin-related protein 1; LPS, lipopolysaccharide; p-, phosphorylated.

Protective effect of rMyonectin against LPS-induced apoptosis and mitochondrial dysfunction in cardiomyocytes is mediated by AMPK activation. Due to the key role of AMPK in energy metabolism, the present study first assessed AMPK activation. Analysis revealed that rMyonectin effectively attenuated the LPS-induced reduction in AMPK phosphorylation in both myocardial tissue and NMCMs (Fig. 7A and B). To determine whether AMPK activation mediates the protective effects of rMyonectin, the present study inhibited AMPK in cardiomyocytes using CC in addition to rMyonectin pretreatment (Fig. 7C).

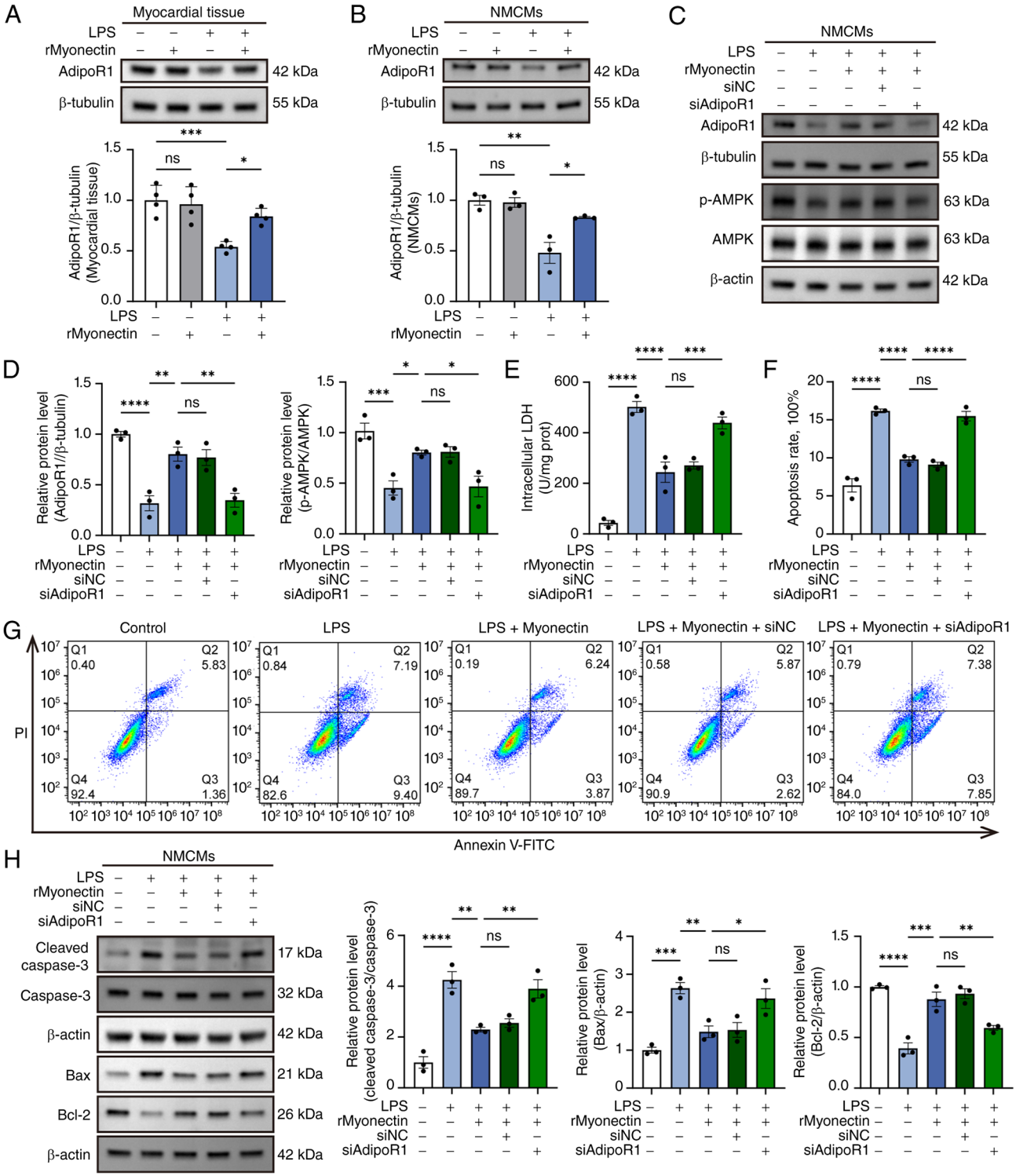

Figure 9. AdipoR1 knockdown abolishes the protective effect of rMyonectin against LPS-induced apoptosis in cardiomyocytes. (A) Western blot analysis and semi-quantification of AdipoR1 in myocardial tissue. (B) Western blot analysis and semi-quantification of AdipoR1 in NMCMs. (C) Representative western blots showing the expression of AdipoR1, p-AMPK and AMPK in NMCMs following AdipoR1 knockdown. (D) Semi-quantification of AdipoR1, p-AMPK and AMPK protein levels in NMCMs following AdipoR1 knockdown. (E) Intracellular LDH activity in NMCMs. (F) The percentage of apoptotic cells detected using flow cytometry. (G) Apoptosis was assessed using flow cytometry after double labeling with Annexin V-FITC and PI. (H) Western blot analysis and semi-quantification of cleaved caspase-3, caspase-3, Bax, and Bcl-2 protein expression in NMCMs. The data are presented as mean±SEM. *P<0.05, **P<0.01, ***P<0.001, ****P<0.0001. rMyonectin, recombinant myonectin; NMCMs, neonatal mouse cardiomyocytes; AdipoR1, adiponectin receptor 1; AMPK, AMP-activated protein kinase; LDH, lactate dehydrogenase; si, small interfering RNA; NC, negative control; siAdipoR1, siRNA targeting AdipoR1; LPS, lipopolysaccharide; p-, phosphorylated; PI, propidium iodide.

CC abolished the protective effects of rMyonectin against cardiomyocyte injury (Fig. 7D) and apoptosis (Fig. 7E-G). Furthermore, CC attenuated the ability of rMyonectin to elevate intracellular ATP levels (Fig. 8A), to increase OCR (Fig. 8B) and activities of mitochondrial respiratory chain complexes I and III (Fig. 8C), and to preserve MMP (Fig. 8D). Western blot analysis

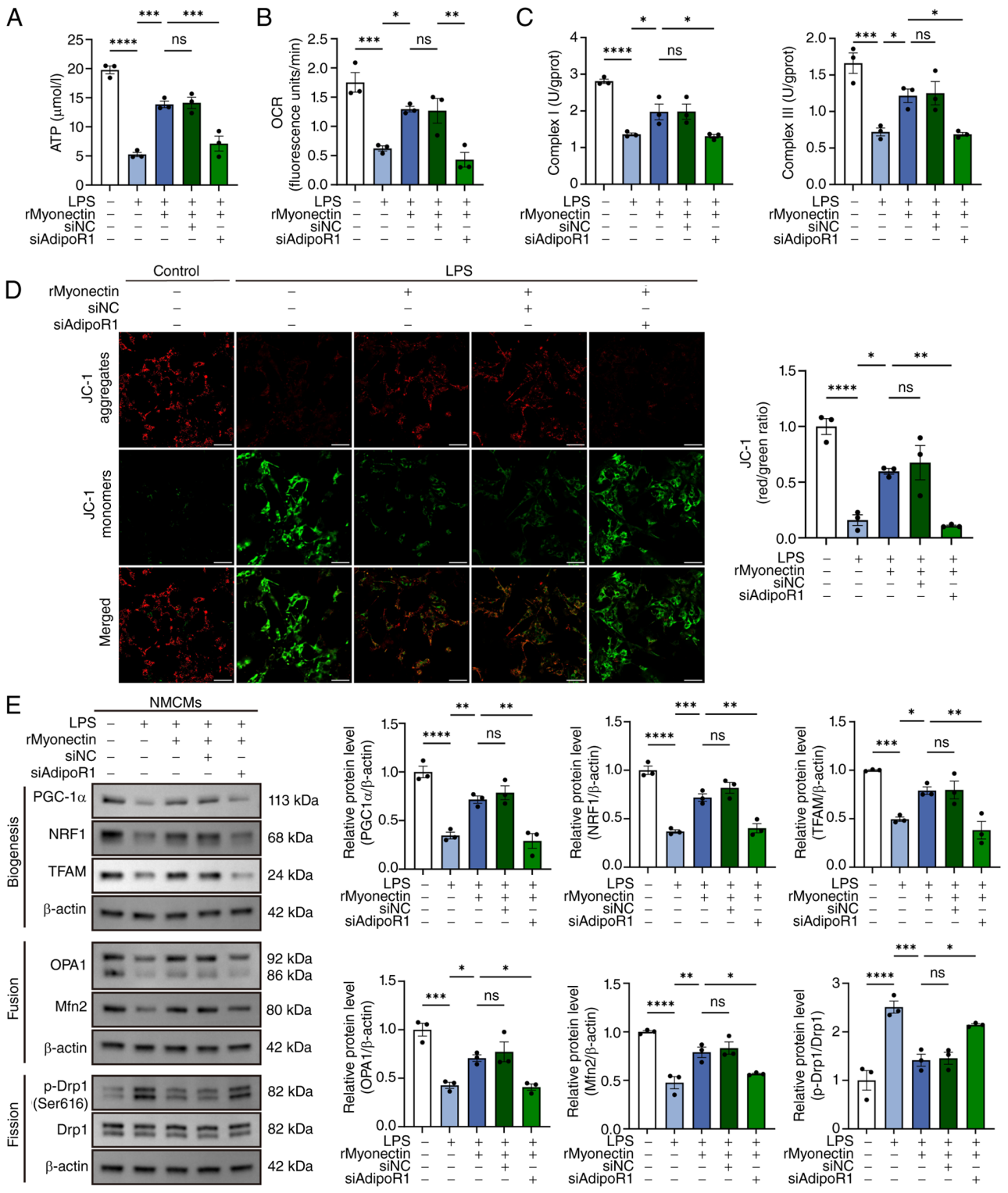

Figure 10. AdipoR1 knockdown abolishes the protective effect of rMyonectin against LPS-induced mitochondrial dysfunction in cardiomyocytes. (A) The ATP content in NMCMs. (B) Relative OCR. (C) Detection of the activities of mitochondrial respiratory chain complexes I and III. (D) Analysis of MMP using JC-1 staining. Scale bar, 50 μm. (E) Western blot analysis and semi-quantification of PGC-1α, NRF1, TFAM, OPA1, Mfn2, p-Drp1 at Ser616 and Drp1 in NMCMs. The data are presented as mean±SEM. *P<0.05, **P<0.01, ***P<0.001, ****P<0.0001. rMyonectin, recombinant myonectin; NMCMs, neonatal mouse cardiomyocytes; AdipoR1, adiponectin receptor 1; AMPK, AMP-activated protein kinase; OCR, oxygen consumption rate; MMP, mitochondrial membrane potential; PGC-1α, peroxisome proliferator-activated receptor γ co-activator-1 α; NRF1, nuclear respiratory factor 1; TFAM, mitochondrial transcription factor A; Mfn2, mitofusin 2; OPA1, optic atrophy 1; Drp1, dynamin-related protein 1; si, small interfering RNA; NC, negative control; siAdipoR1, siRNA targeting AdipoR1; LPS, lipopolysaccharide; p-, phosphorylated.

further demonstrated that the rMyonectin-induced upregulation of PGC-1α, NRF1, TFAM, OPA1 and Mfn2, as well as the downregulation of the p-Drp1(Ser616)/Drp1 ratio, was abolished upon AMPK inhibition (Fig. 8E). These results demonstrate that the anti-apoptotic and mitochondrial-protective effects of rMyonectin are mediated by AMPK activation.

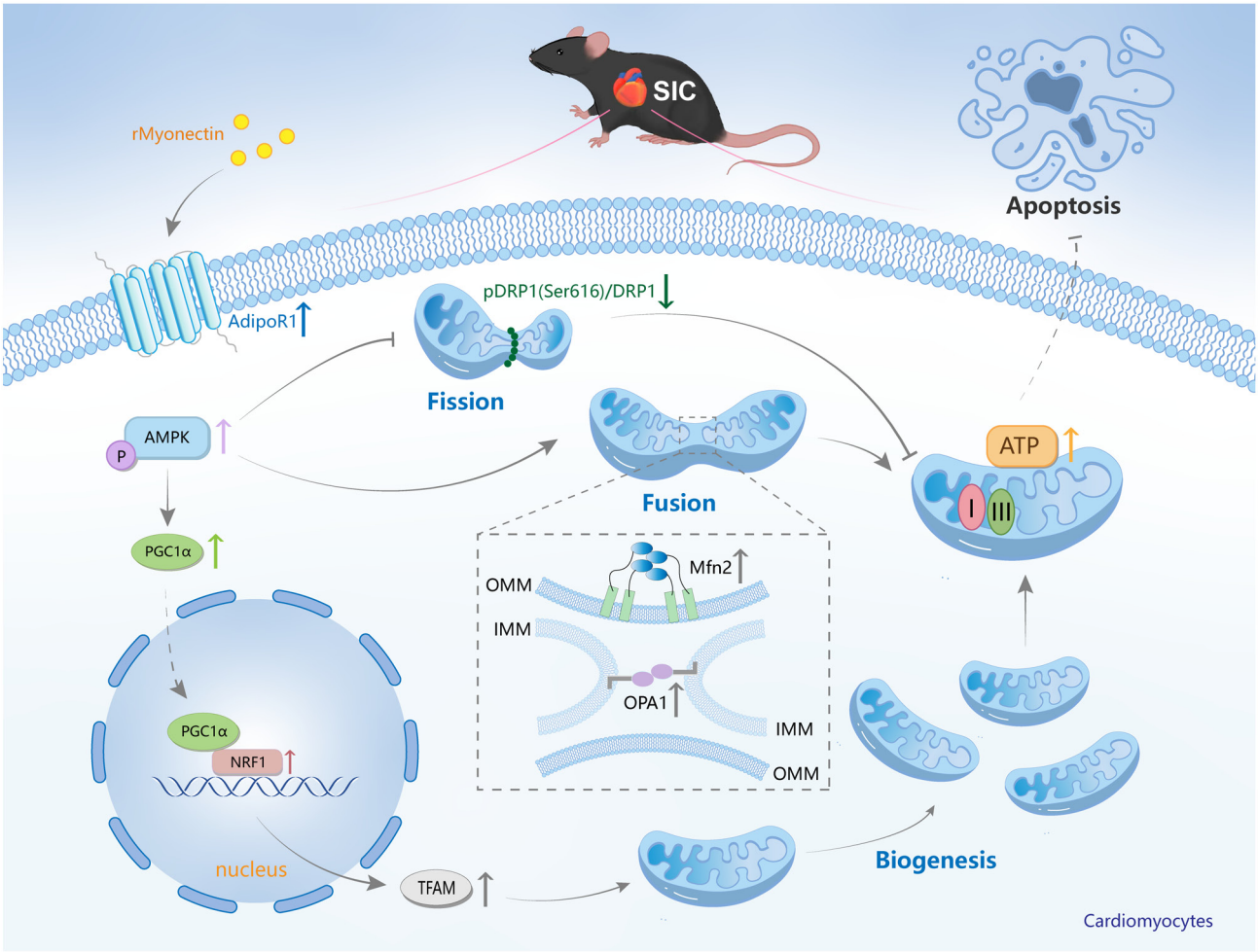

Figure 11. Molecular mechanism by which rMyonectin ameliorates SIC. rMyonectin ameliorates SIC by alleviating mitochondrial dysfunction and inhibiting cardiomyocyte apoptosis via activation of the AdipoR1/AMPK pathway. rMyonectin, recombinant myonectin; SIC, sepsis-induced cardiomyopathy; OMM, outer mitochondrial membranes; IMM, inner mitochondrial membranes; AdipoR1, adiponectin receptor 1; AMPK, AMP-activated protein kinase; PGC-1α, peroxisome proliferator-activated receptor γ co-activator-1 α; NRF1, nuclear respiratory factor 1; TFAM, mitochondrial transcription factor A; Mfn2, mitofusin 2; OPA1, optic atrophy 1; Drp1, dynamin-related protein 1; I, mitochondrial respiratory chain complex I; III, mitochondrial respiratory chain complex III; p-, phosphorylated.

AdipoR1 knockdown abolishes the protective effect of rMyonectin against LPS-induced apoptosis and mitochondrial dysfunction in cardiomyocytes. Myonectin is a paralog of adiponectin, sharing similar structural and functional characteristics. Adiponectin mediates its cardioprotective effects primarily through activating the adiponectin receptors. Notably, AdipoR1 has been established as an upstream activator in the AMPK signaling pathway (31,32). To determine whether myonectin protected cardiomyocytes through the AdipoR1/AMPK pathway, the present study measured AdipoR1 protein levels in myocardial tissue and NMCMs. The results indicated that rMyonectin treatment reversed the LPS-induced downregulation of AdipoR1 expression in these models (Fig. 9A and B). Following siRNA-mediated knockdown of AdipoR1 in NMCMs (with transfection efficiency validated in Figs. S1 and S2), AMPK phosphorylation was reduced (Fig. 9C and D), and the protective effects of rMyonectin were abolished. Specifically, AdipoR1 knockdown reversed the protective effects of rMyonectin against cardiomyocyte injury (Fig. 9E) and apoptosis (Fig. 9F-H). Moreover, it eliminated the rMyonectin-induced enhancements in intracellular ATP levels (Fig. 10A), OCR (Fig. 10B), the activities of mitochondrial respiratory chain complexes I and III (Fig. 10C), as well as the restoration of MMP (Fig. 10D). Western blot analysis further demonstrated that the rMyonectin-induced upregulation of PGC-1α, NRF1, TFAM, OPA1 and Mfn2, as well as the downregulation of the p-Drp1(Ser616)/Drp1 ratio, was abolished by AdipoR1 knockdown (Fig. 10E). Collectively, these results demonstrate that rMyonectin protects cardiomyocytes from LPS-induced injury via the AdipoR1/AMPK pathway.

Discussion

To the best of our knowledge, the present study elucidated, for the first time, the protective role of rMyonectin in SIC by using both LPS- and CLP-induced *in vivo* models, together with LPS-stimulated cardiomyocytes for *in vitro* validation. Mechanistically, rMyonectin exerted its cardioprotective effects by activating the AdipoR1/AMPK pathway, which in turn ameliorated mitochondrial dysfunction (as evidenced by enhanced mitochondrial biogenesis, restored homeostasis of mitochondrial dynamics, increased OCR, elevated activities

of mitochondrial respiratory chain complexes I and III and enhanced ATP production) and suppressed cardiomyocyte apoptosis (Fig. 11). Collectively, these findings suggest that rMyonectin holds promise as a protective candidate for SIC.

Myonectin, also known as CTRP15, is a member of the CTRP family. The CTRPs are paralogs of adiponectin and serve diverse roles in metabolism and cardiovascular physiology. The majority of CTRPs, with the exception of CTRP4, share a common structure composed of four distinct domains: A signal peptide at the N terminus, a short variable region, a collagenous domain and a C-terminal globular domain that is homologous to C1q. Despite this common architectural framework, individual CTRPs exhibit distinct tissue specific expression profiles and regulate a wide array of physiological functions (31). The heart not only expresses several members of the CTRPs but also serves as an important target organ for their actions (33). Given this, their roles in cardiac pathologies such as SIC are of substantial interest. Accumulating evidence has elucidated the roles and underlying mechanisms of CTRPs in SIC. For instance, Wei *et al* (34) revealed that CTRP3 expression was upregulated in cardiac tissue upon LPS stimulation. CTRP3 protected against sepsis-induced cardiac dysfunction by activating the AMPKα pathway, thereby inhibiting inflammatory responses and apoptosis. Similarly, CTRP1 has been shown to exert a protective effect against LPS-induced cardiac injury through a sirtuin 1-dependent mechanism that attenuates oxidative stress and inflammation (25). CTRP9 also protects against LPS-induced acute myocardial injury by inhibiting the inflammatory response via an AdipoR1/AMPK-dependent pathway (35).

Myonectin is a myokine primarily synthesized and secreted by skeletal muscle and is also expressed in cardiac and smooth muscle. Exercise stimulates the upregulation of myonectin in skeletal muscle and increases its circulating concentration (36). To date, its precise functions and mechanisms in cardiovascular diseases remain poorly characterized. Otaka *et al* (17) systematically elucidated the role of myonectin in myocardial I/R injury using a multifaceted experimental approach that included generating myonectin-knockout mice, performing AAV-mediated knockdown of myonectin in skeletal muscle, and administering rMyonectin intravenously. They found that skeletal muscle-derived myonectin protected against myocardial I/R injury in mice by suppressing the inflammatory response in macrophages and apoptosis in cardiomyocytes through the S1P/cAMP/Akt signaling pathway. Zhao *et al* (18) demonstrated that myonectin exhibited markedly higher expression in cardiomyocytes compared with cardiac fibroblasts. The study further revealed that myonectin attenuated myocardial fibrosis by promoting the phosphorylation of the IR and IRS-1, thereby activating the PI3K/Akt signaling pathway. These findings establish myonectin as a functionally relevant factor in cardiovascular pathophysiology. To investigate the role of myonectin in SIC, the present study employed two complementary murine models (intraperitoneal LPS challenge and CLP) together with LPS-challenged NMCMs for *in vitro* validation, with rMyonectin administered accordingly. The results consistently demonstrated that rMyonectin effectively ameliorated cardiac dysfunction *in vivo*, and reduced myocardial injury as well as suppressed cardiomyocyte apoptosis in both *in vivo* and *in vitro* settings, collectively validating its cardioprotective effect.

To investigate the potential mechanisms of myonectin in the heart, the present study drew an analogy based on its known functions in skeletal muscle. Existing literature indicated that in skeletal tissue, myonectin activated the AMPK/PGC-1α signaling pathway, promoted mitochondrial biogenesis, and thus ameliorated mitochondrial dysfunction (19). Mitochondrial dysfunction serves as an important pathogenic mechanism underlying SIC. This dysfunction is characterized by structural abnormalities, oxidative stress, altered mitochondrial permeability, mitochondrial uncoupling and dysregulation of mitochondrial quality control systems along with disrupted calcium homeostasis (37,38). Mitochondrial quality control is maintained through three interconnected processes: Dynamics (fusion and fission), biogenesis and mitophagy (39). Under physiological conditions, a continuous cycle of fusion and fission sustains mitochondrial structural integrity and functional homeostasis. Fission and fusion are indispensable for a range of key cellular functions, including ATP production, mitochondrial DNA (mtDNA) distribution, mitochondrial respiratory activity, cell survival, apoptosis and calcium signaling (40). Fusion of the outer and inner mitochondrial membranes is primarily mediated by mitofusins (Mfn1/2) and OPA1, respectively. Mitochondrial fusion enables the dynamic repair of reversibly damaged portions of mitochondria, forming functional elongated organelles (41).

Mitochondrial fission is a process whereby Drp1 triggers constriction of the mitochondrial membrane, resulting in the division of a single mitochondrion into two separate organelles (40). Phosphorylation of Drp1 at serine 616 is an activating modification that drives its recruitment to the outer mitochondrial membranes, leading to mitochondrial fragmentation (42). A homeostatic balance between mitochondrial fusion and fission is essential for maintaining mitochondrial network integrity and ensuring proper cellular physiological function. In septic mice, myocardial Drp1 activation and Mfn2 downregulation promote a pathological shift toward mitochondrial fission, leading to an imbalance in mitochondrial dynamics and, ultimately, to mitochondrial dysfunction and apoptosis (8,37). Mitochondrial biogenesis can be defined as the growth and division of pre-existing mitochondria (43), which requires coordinated mtDNA replication and expression, import of nuclear-encoded proteins, and phospholipid transport for membrane assembly (44). PGC-1α is the primary regulator of mitochondrial biogenesis. It co-activates NRF1, which in turn activates the promoter of TFAM. Through this transcriptional cascade, PGC-1α mediates the expression of mitochondrial proteins encoded by both nuclear DNA and mtDNA, promoting mitochondrial biogenesis, regulating the intracellular mitochondrial content, increasing mitochondrial ATP production and coordinating cellular energy metabolism (45). The findings of the present study indicate that rMyonectin protects against SIC by activating the AMPK pathway, which upregulates PGC-1α, NRF1, TFAM, OPA1 and Mfn2, while downregulating p-Drp1(Ser616)/Drp1, thereby restoring the myocardial mitochondrial fission-fusion balance and promoting mitochondrial biogenesis. The present study provides the first evidence that myonectin regulates mitochondrial dynamics.

How myonectin activates AMPK to alleviate mitochondrial dysfunction warrants further investigation. Notably, the specific receptors for adiponectin, AdipoR1 and AdipoR2, mediate AMPK and PPARα activation, respectively (32). Koentges *et al* (14) showed that loss of AdipoR1 induced cardiac mitochondrial dysfunction and uncoupling in mice, a phenotype not observed with AdipoR2 loss. Given that myonectin is a paralog of adiponectin, the two proteins share structural similarities (31). This led to the investigation of whether myonectin acts through a similar receptor-mediated pathway. Having demonstrated that myonectin activated the AMPK pathway, we hypothesized that AdipoR1 mediated the protective effects of myonectin in SIC. The present data confirmed this hypothesis, as AdipoR1 knockdown abolished the protective effects of rMyonectin on mitochondrial dysfunction and cardiomyocyte apoptosis in NMCMs.

Several limitations of the present study should be acknowledged. First, rMyonectin was administered systemically via tail vein injection. This non-targeted delivery resulted in its broad distribution across multiple tissues and organs, which confounded the interpretation of its cardiac-specific effects *in vivo*. Consequently, the cardiac specificity of myonectin in SIC remains to be elucidated in future studies. Second, the present study employed a pretreatment protocol, which is a classic design in mechanistic research to elucidate the protective effects and signaling pathways of rMyonectin. However, this prophylactic administration protocol is not fully aligned with real-world clinical practice, and the present study did not evaluate the efficacy of therapeutic administration. Future studies are warranted to further assess the therapeutic efficacy of rMyonectin when administered after the onset of sepsis, in order to determine its potential for clinical translation. Finally, the *in vivo* experiments in the present study were conducted exclusively in male mice, a long-standing convention in cardiovascular basic research. The primary rationale for this approach was to avoid potential interference of the female estrous cycle with cardiac contractile function. Although a study has suggested that under conventional group-housing conditions the estrous cycle in female mice may be irregular, thereby reducing such interference to some extent (46), the influence of the estrous cycle on cardiac function cannot be completely excluded. Nevertheless, the exclusive use of male mice in this design inevitably introduces a sex-specific bias, limiting the generalizability across sexes. Future studies should repeat the key experiments in female mice to assess the impact of sex on the results.

In conclusion, the present study demonstrates that rMyonectin protects against SIC by activating AdipoR1/AMPK signaling, thereby restoring mitochondrial function and suppressing apoptosis to alleviate cardiac injury and dysfunction. These findings position rMyonectin as a novel and promising protective agent for SIC.

Acknowledgements

We are grateful to the following colleagues from the Scientific Research Center of China-Japan Union Hospital of Jilin University for their guidance and support with flow cytometry: Dr Yucheng Zhang, Ms. Yingnan Liu (lab technician), Ms. Huiying Lv (lab technician) and Ms. Puyu Gao (lab technician).

Funding

The present study was supported by the National Natural Science Foundation of China (grant nos. 82470327 and 82470400) and the Project of Jilin Provincial Department of Finance (grant no. 2022SCZ40).

Availability of data and materials

The data generated in the present study may be requested from the corresponding author.

Authors' contributions

PL contributed to study design, data analysis and manuscript drafting. RC, HZ, HL and LL contributed to study design and conducted the initial data interpretation. BD and PY contributed to study design, critical review and manuscript revision. All authors reviewed the manuscript critically. BD and PY confirm the authenticity of all the raw data. All authors read and approved the final version of the manuscript.

Ethics approval and consent to participate

All animal procedures were approved by the Institutional Ethics Committee of the School of Basic Medical Sciences, Jilin University (approval nos. 2025-597 and 2026-491).

Patient consent for publication

Not applicable.

Competing interests

The authors declare that they have no competing interests.

References

1. Aissaoui N, Boissier F, Chew M, Singer M and Vignon P: Sepsis-induced cardiomyopathy. Eur Heart J 46: 3339-3353, 2025.
2. Lanspa MJ, Cirulis MM, Wiley BM, Olsen TD, Wilson EL, Beesley SJ, Brown SM, Hirshberg EL and Grissom CK: Right ventricular dysfunction in early sepsis and septic shock. Chest 159: 1055-1063, 2021.
3. Kuroshima T, Kawaguchi S and Okada M: Current perspectives of mitochondria in sepsis-induced cardiomyopathy. Int J Mol Sci 25: 4710, 2024.
4. Liu YC, Yu MM, Shou ST and Chai YF: Sepsis-induced cardiomyopathy: Mechanisms and treatments. Front Immunol 8: 1021, 2017.
5. Stanzani G, Duchen MR and Singer M: The role of mitochondria in sepsis-induced cardiomyopathy. Biochim Biophys Acta Mol Basis Dis 1865: 759-773, 2019.
6. Lopaschuk GD, Karwi QG, Tian R, Wende AR and Abel ED: Cardiac energy metabolism in heart failure. Circ Res 128: 1487-1513, 2021.
7. Suliman HB, Welty-Wolf KE, Carraway M, Tatro L and Piantadosi CA: Lipopolysaccharide induces oxidative cardiac mitochondrial damage and biogenesis. Cardiovasc Res 64: 279-288, 2004.
8. Chen XS, Cui JR, Meng XL, Wang SH, Wei W, Gao YL, Shou ST, Liu YC and Chai YF: Angiotensin-(1-7) ameliorates sepsis-induced cardiomyopathy by alleviating inflammatory response and mitochondrial damage through the NF-κB and MAPK pathways. J Transl Med 21: 2, 2023.

9. Zhang S, Xu Y, Zhu J, Ma J, Niu Q and Wang X: Carbon monoxide attenuates LPS-induced myocardial dysfunction in rats by regulating the mitochondrial dynamic equilibrium. Eur J Pharmacol 889: 173726, 2020.
10. Chen XS, Wang SH, Liu CY, Gao YL, Meng XL, Wei W, Shou ST, Liu YC and Chai YF: Losartan attenuates sepsis-induced cardiomyopathy by regulating macrophage polarization via TLR4-mediated NF-κB and MAPK signaling. Pharmacol Res 185: 106473, 2022.
11. Kim TT and Dyck JR: Is AMPK the savior of the failing heart? Trends Endocrinol Metab 26: 40-48, 2015.
12. Wan S, Cui Z, Wu L, Zhang F, Liu T, Hu J, Tian J, Yu B, Liu F, Kou J and Li F: Ginsenoside Rd promotes omentin secretion in adipose through TBK1-AMPK to improve mitochondrial biogenesis via WNT5A/Ca^{2+} pathways in heart failure. Redox Biol 60: 102610, 2023.
13. Jin Z, Li X, Liu H, He T, Jiang W, Peng L, Wu X, Chen M, Fan Y, Lu Z, *et al*: MEGF9 prevents lipopolysaccharide-induced cardiac dysfunction through activating AMPK pathway. Redox Rep 30: 2435252, 2025.
14. Koentges C, König A, Pfeil K, Hölscher ME, Schnick T, Wende AR, Schrepper A, Cimolai MC, Kersting S, Hoffmann MM, *et al*: Myocardial mitochondrial dysfunction in mice lacking adiponectin receptor 1. Basic Res Cardiol 110: 37, 2015.
15. Petro JL, Gallo-Villegas J and Calderón JC: Myonectin and metabolic health: A systematic review. Front Endocrinol (Lausanne) 16: 1557142, 2025.
16. Srole DN and Ganz T: Erythroferrone structure, function, and physiology: Iron homeostasis and beyond. J Cell Physiol 236: 4888-4901, 2021.
17. Otaka N, Shibata R, Ohashi K, Uemura Y, Kambara T, Enomoto T, Ogawa H, Ito M, Kawanishi H, Maruyama S, *et al*: Myonectin is an exercise-induced myokine that protects the heart from ischemia-reperfusion injury. Circ Res 123: 1326-1338, 2018.
18. Zhao Q, Zhang CL, Xiang RL, Wu LL and Li L: CTRP15 derived from cardiac myocytes attenuates TGFβ1-induced fibrotic response in cardiac fibroblasts. Cardiovasc Drugs Ther 34: 591-604, 2020.
19. Ozaki Y, Ohashi K, Otaka N, Kawanishi H, Takikawa T, Fang L, Takahara K, Tatsumi M, Ishihama S, Takefuji M, *et al*: Myonectin protects against skeletal muscle dysfunction in male mice through activation of AMPK/PGC1α pathway. Nat Commun 14: 4675, 2023.
20. Saiyang X, Qingqing W, Man X, Chen L, Min Z, Yun X, Wenke S, Haiming W, Xiaofeng Z, Si C, *et al*: Activation of Toll-like receptor 7 provides cardioprotection in septic cardiomyopathy-induced systolic dysfunction. Clin Transl Med 11: e266, 2021.
21. Ni L, Lin B, Shen M, Li C, Hu L, Fu F, Chen L, Yang J and Shi D: PKM2 deficiency exacerbates gram-negative sepsis-induced cardiomyopathy via disrupting cardiac calcium homeostasis. Cell Death Discov 8: 496, 2022.
22. Fang Y, Yang B, Zhu D, Zhang X, Jiang X, Wang H, Zhang L, Yu Y, Yang Y, Yuan M, *et al*: Anemoside B4 ameliorates septic cardiomyopathy by activating SRC-mediated PI3K/AKT/mTOR pathway to alleviate mitochondrial dysfunction and cardiomyocyte senescence. Int Immunopharmacol 171: 116108, 2026.
23. Yang B, Li T, Wang Z, Zhu Y, Niu K, Hu S, Lin Z, Zheng X, Jin X and Shen C: Ruxolitinib-based senomorphic therapy mitigates cardiomyocyte senescence in septic cardiomyopathy by inhibiting the JAK2/STAT3 signaling pathway. Int J Biol Sci 20: 4314-4340, 2024.
24. Wan TT, Li Y, Li JX, Xiao X, Liu L, Li HH and Guo SB: ACE2 activation alleviates sepsis-induced cardiomyopathy by promoting MasR-Sirt1-mediated mitochondrial biogenesis. Arch Biochem Biophys 752: 109855, 2024.
25. Jiang W, Li W, Hu X, Hu R, Li B and Lan L: CTRP1 prevents sepsis-induced cardiomyopathy via Sirt1-dependent pathways. Free Radic Biol Med 152: 810-820, 2020.
26. Ravi V, Jain A, Taneja A, Chatterjee K and Sundaresan NR: Isolation and culture of neonatal murine primary cardiomyocytes. Curr Protoc 1: e196, 2021.
27. Wang H, Wang L, Hu F, Wang P, Xie Y, Li F and Guo B: Neuregulin-4 attenuates diabetic cardiomyopathy by regulating autophagy via the AMPK/mTOR signalling pathway. Cardiovasc Diabetol 21: 205, 2022.
28. Yang F, Qin Y, Wang Y, Meng S, Xian H, Che H, Lv J, Li Y, Yu Y, Bai Y and Wang L: Metformin inhibits the NLRP3 inflammasome via AMPK/mTOR-dependent effects in diabetic cardiomyopathy. Int J Biol Sci 15: 1010-1019, 2019.
29. Wang J, Pu X, Zhuang H, Guo Z, Wang M, Yang H, Li C and Chang X: Astragaloside IV alleviates septic myocardial injury through DUSP1-Prohibitin 2 mediated mitochondrial quality control and ER-autophagy. J Adv Res 75: 561-580, 2025.
30. Livak KJ and Schmittgen TD: Analysis of relative gene expression data using real-time quantitative PCR and the 2(-delta delta C(T)) method. Methods 25: 402-408, 2001.
31. Schäffler A and Buechler C: CTRP family: Linking immunity to metabolism. Trends Endocrinol Metab 23: 194-204, 2012.
32. Nguyen TMD: Adiponectin: Role in physiology and pathophysiology. Int J Prev Med 11: 136, 2020.
33. Schanbacher C, Hermanns HM, Lorenz K, Wajant H and Lang I: Complement 1q/tumor necrosis factor-related proteins (CTRPs): Structure, receptors and signaling. Biomedicines 11: 559, 2023.
34. Wei WY, Ma ZG, Zhang N, Xu SC, Yuan YP, Zeng XF and Tang QZ: Overexpression of CTRP3 protects against sepsis-induced myocardial dysfunction in mice. Mol Cell Endocrinol 476: 27-36, 2018.
35. Kambara T, Shibata R, Ohashi K, Matsuo K, Hiramatsu-Ito M, Enomoto T, Yuasa D, Ito M, Hayakawa S, Ogawa H, *et al*: C1q/tumor necrosis factor-related protein 9 protects against acute myocardial injury through an adiponectin receptor I-AMPK-dependent mechanism. Mol Cell Biol 35: 2173-2185, 2015.
36. Seldin MM, Peterson JM, Byerly MS, Wei Z and Wong GW: Myonectin (CTRP15), a novel myokine that links skeletal muscle to systemic lipid homeostasis. J Biol Chem 287: 11968-11980, 2012.
37. Lin Y, Xu Y and Zhang Z: Sepsis-induced myocardial dysfunction (SIMD): The pathophysiological mechanisms and therapeutic strategies targeting mitochondria. Inflammation 43: 1184-1200, 2020.
38. Sato R, Sanfilippo F, Lanspa M, Duggal A and Dugar S: Sepsis-induced cardiomyopathy: Mechanism, prevalence, assessment, prognosis, and management. Chest 168: 1383-1394, 2025.
39. Liu BH, Xu CZ, Liu Y, Lu ZL, Fu TL, Li GR, Deng Y, Luo GQ, Ding S, Li N and Geng Q: Mitochondrial quality control in human health and disease. Mil Med Res 11: 32, 2024.
40. Jin JY, Wei XX, Zhi XL, Wang XH and Meng D: Drp1-dependent mitochondrial fission in cardiovascular disease. Acta Pharmacol Sin 42: 655-664, 2021.
41. Forte M, Schirone L, Ameri P, Basso C, Catalucci D, Modica J, Chimenti C, Crotti L, Frati G, Rubattu S, *et al*: The role of mitochondrial dynamics in cardiovascular diseases. Br J Pharmacol 178: 2060-2076, 2021.
42. Serasinghe MN and Chipuk JE: Mitochondrial fission in human diseases. Handb Exp Pharmacol 240: 159-188, 2017.
43. Jornayvaz FR and Shulman GI: Regulation of mitochondrial biogenesis. Essays Biochem 47: 69-84, 2010.
44. Liu L, Li Y, Chen G and Chen Q: Crosstalk between mitochondrial biogenesis and mitophagy to maintain mitochondrial homeostasis. J Biomed Sci 30: 86, 2023.
45. Murphy MP and Hartley RC: Mitochondria as a therapeutic target for common pathologies. Nat Rev Drug Discov 17: 865-886, 2018.
46. MacDonald JK, Pyle WG, Reitz CJ and Howlett SE: Cardiac contraction, calcium transients, and myofilament calcium sensitivity fluctuate with the estrous cycle in young adult female mice. Am J Physiol Heart Circ Physiol 306: H938-H953, 2014.